# DEVELOPMENT OF TRANSPARENT SUPERHYDROPHOBIC AND SELF-CLEANING SURFACES

BY

MUHAMMAD RIZWAN YOUSAF

A Thesis Presented to the
DEANSHIP OF GRADUATE STUDIES

**KING FAHD UNIVERSITY OF PETROLEUM & MINERALS**

DHAHRAN, SAUDI ARABIA

In Partial Fulfillment of the
Requirements for the Degree of

# MASTER OF SCIENCE

**In**

MECHANICAL ENGINEERING

Jan 2017

KING FAHD UNIVERSITY OF PETROLEUM & MINERALS

DHAHRAN- 31261, SAUDI ARABIA

**DEANSHIP OF GRADUATE STUDIES**

This thesis, written by **MUHAMMAD RIZWAN YOUSAF** under the direction his thesis advisor and approved by his thesis committee, has been presented and accepted by the Dean of Graduate Studies, in partial fulfillment of the requirements for the degree of **MASTER OF SCIENCE IN MECHANICAL ENGINEERING.**

Dr. Bekir Sami Yilbas
(Advisor)

Dr. Zuhair M. Gasem
Department Chairman

Dr. Mazen Mohamad Khaled
(Member)

Dr. Salam A. Zummo
Dean of Graduate Studies

Dr. Numan Abu-Dheir
(Member)

12/2/17
Date

*Dedication*

**To my parents for their endless love**

# ACKNOWLEDGMENTS

I would like to express my sincere gratitude to Dr. Bekir Sami Yilbas for supervising my Master's Thesis. It has truly been a great learning experience for me. I would like to thank him for his suggestions, guidance, and support during the course of my research.

I would like to appreciate the support and help I received from Dr. Mazen Khaled to carry out some of my research work in Chemistry Department. I am thankful to my committee members, Dr-Numan Abu Dheir and Dr. Mazen Khaled, for their valuable input in my thesis work.

I would also like to thank other members of our research group, Dr. Haider and Dr. Abdullah for their tremendous help in research related work.

I am grateful to my all my friends, especially Mr.Sharjeel Javid and Mr. Syed Haris Iftikhar for all the happy and joyful moments.

Finally, I would like to dedicate this thesis to my parents. I owe everything to them.

# TABLE OF CONTENTS

# LIST OF TABLES

# LIST OF FIGURES

# LIST OF ABBREVIATIONS

| | | |
|---|---|---|
| **C.A** | : | Contact Angle |
| **CAH** | : | Contact Angle Hysteresis |
| **OTS** | : | Octadecyltrichlorosilane |
| **PDMS** | : | Polydimethylsiloxane |
| **PFOTS** | : | Trichloro(1H,1H,2H,2H-perfluorooctyl |
| **WCA** | : | Water Contact Angle |

# ABSTRACT

Full Name : [Muhammad Rizwan Yousaf]

Thesis Title : [Development of Transparent Superhydrophobic and Self-Cleaning Surfaces]

Major Field : [Mechanical Engineering]

Date of Degree : [Jan 2017]

Wetting characteristics of surfaces are influenced by both, the surface texture and the surface energy of substrate materials. Surfaces consisting of a hierarchal texture covered with a low surface energy material show unusual water repellency and are termed as superhydrophobic surfaces. A water droplet on such surface rolls off at small inclination angles, and picks and carries away small particles along its path, thereby, giving rise to the self-cleaning effect. These surfaces have attracted considerable attention in recent years due to their vast technological applications ranging from self-cleaning windows, textiles, and paints to low drag surfaces for energy conversion.

Replication of textured surfaces by PDMS (Polydimethylsiloxane) is introduced as a fast and cost effective way of making optically transparent superhydrophobic surfaces. Laser textured alumina tiles and photo lithographically etched silicon wafers are used as templates for replication studies. Surfaces obtained by replicating laser textured alumina tiles exhibit smaller water contact angles (less than 150°) due to the absence of nano-sized whisker like structures. Functionalized silica nanoparticles are, therefore, introduced at the replicated PDMS surfaces to make them superhydrophobic (water contact angle ≥150°). Surfaces obtained by replicating etched silicon wafers, on the other hand, are superior in terms of superhydrophobic characteristics and optical transmittance.

A facile approach to render conventional glass surfaces superhydrophobic is through silica nanoparticle coating. Functionalized silica nanoparticles are synthesized and deposited onto the glass workpieces. The surfaces, thus obtained, give water contact angles exceeding 170° with an average optical transmittance of 67.22%. Improvement in optical transmittance is brought about by using the process of convective assembly to get a thin layer of silica nanoparticles at the glass surface.

Impregnating the texture of a superhydrophobic surface by some lubricant oil is a relatively new concept that is used to impart some beneficial properties to superhydrophobic surfaces. The criterion governing the formation of a stable lubricant oil film on a textured surface is highlighted and oil impregnated surfaces are prepared in accordance with the oil film stability criterion. The last part of the thesis focuses on the characterization of dust particles, collected from Dhahran area, via using advanced analysis techniques.

# ملخص الرسالة

**الاسم الكامل** : **محمد رضوان يوسف**

**عنوان الرسالة** : **تطوير أسطح شفافة نافرة جداً من الماء لغرض التنظيف الذاتي**

**التخصص** : **الهندسة الميكانيكية**

**تاريخ الدرجة العلمية: يناير 2017**

خصائص ترطيب السطوح تتأثر على حد سواء بنسيج وطاقة الأسطح للمواد الركيزة. الأسطح التي تتكون من نسيج هرمي مغطى بمادة طاقتها السطحية منخفضة تظهر نفورًا غير عاديًا للمياه ، مما يطلق عليها الأسطح النافرة للمياة. قطرات الماء على هذه الأسطح تتدحرج عند ميلان السطح بزوايا صغيرة، وتلتقط وتحمل بعيدًا الجزيئات الصغيرة على طول مسارها، مما يؤدي إلى حدوث تأثير التنظيف الذاتي. أجتذبت هذه الأسطح اهتمامًا كبيرًا في السنوات الأخيرة بسبب تطبيقاتها التكنولوجية الواسعة والتي تتراوح من التنظيف الذاتي للنوافذ والمنسوجات والدهانات إلى أسطح منخفضة طاقة السحب لغرض تحوّلات الطاقة.

يتم في هذه الرسالة طرح عملية نسخ الأسطح النافرة للمياه بواسطة ثنائي ميثيل بولي سيلوكسان (PDMS) باعتبارها وسيلة سريعة وفعالة من حيث التكلفة لإنتاج أسطح نافرة للمياة وشفافة بصريًا. استخدمت رقائق الألومينا محفورة بالليزر ورقائق السيليكون المحفورة بتقنية الليثيوجرافك كقوالب لإجراء دراسات إنتاج النسخ. الأسطح الناتجة من استخدام رقائق الالومينا المحفورة بالليزر أبدت زوايا ملامسة للماء صغيرة (أقل من 150 درجة) نظرًا لعدم وجود هياكل نانوية طولية. لذلك، تم إضافة جزيئات السيليكا النانوية المطورة لأسطح ال **(PDMS)** لجعلها أسطح نافرة للمياه (زاوية ملامسة الماء $\geq$ 150 درجة). بالجهة المقابلة، أبدت الأسطح الناتجة من استخدام رقائق السيليكون المحفورة تفوق أعلى من ناحية خصائص الأسطح النافرة للمياه والنفاذية البصرية.

وهناك نهج سطحي وتجريبي لتقديم أسطح الزجاج التقليدية النافرة للمياه وذلك من خلال الطلاء بجزيئات السيليكا النانوية. تم تطوير جزيئات السيليكا النانوية ووضعت على قطع الزجاج التجريبية. وبذلك، أبدت الأسطح زوايا ملامسة للماء تتعدى ال 170 درجة ومعدل نفاذية بصرية بمقدار 67.22 %. طوّرت النفاذية البصرية لهذه الأسطح عن طريق طلائها بغمسها في محلول خاص لإستخراج طبقات رقيقة من جزيئات السيليكا النانوية

تعبئة هذه الأسطح بالزيت هو مفهوم جديد نسبيًا يستخدم لإضافة بعض الخصائص المفيدة للأسطح النافرة للمياه. وقد سلط الضوء في هذه الرسالة على المعيار الذي يحكم تشكيل طبقة مستقرة من زيت التشحيم على الأسطح وتم إعداد الأسطح المعبئة بالزيت وفقًا لمعيار إستقرار طبقة الزيت. وفي الجزء الأخير من الرسالة، تم توصيف خصائص جزيئات غبار جمعت من منطقة الظهران باستخدام تقنيات تحليل متقدمة.

# CHAPTER 1

# INTRODUCTION

Wetting characteristics of surfaces play an important role in many of the processes involving liquid/surface interactions [1].Development of surfaces with enhanced wetting/non-wetting characteristics to meet required applications has received a great deal of attention in recent years both from industry and academia [2]-[3].The chemical nature of a surface and its texture characteristics can both be adjusted to allow the surfaces to be used in self-cleaning [4], anti-biofouling [5], anti-smudge [6], anti-fog [7] and low-drag applications [8]. Self-cleaning surfaces with high optical transmittance are of special interest because of their wide range of applications e.g. windows for skyscrapers, protective covers for PV-panels, windshield of cars and etc. The required effort to remove the dust particles from such surfaces is considerably reduced. This, in turn, lowers the costs associated with the cleaning of conventional wetting surfaces.

In order to explore the surface wetting phenomenon, it is important to highlight some of the properties that govern the wettability of surfaces.

## 1.1 Theoretical Background

Wetting of surfaces is a complex phenomenon, influenced not only by the surface energies of the relevant phases, but by the surface texture of the solid substrate as well. In the coming sections, some theoretical background for droplet behavior on smooth and rough surfaces

will be presented. For the case of droplets on rough surfaces, two different states, wenzel and cassie-bexter will be discussed. It will be followed by a brief overview of lubricant impregnated surfaces.

### 1.1.1 Wetting on Smooth Surfaces

A surface's wettability is most often expressed by the contact angle (C.A). It is defined as the angle formed between the solid/liquid interface and the liquid/vapor interface when a droplet is placed on a surface. This has been illustrated in Figure 1.1.

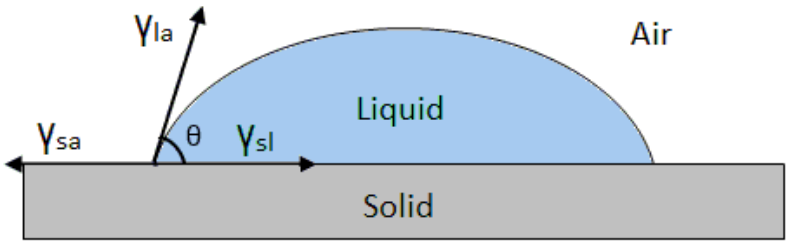


Figure 1.1 Force balance of interfacial tensions at three phase contact line

The contact angle is dictated by the equilibrium of the interfacial tensions at the three phase contact line. i.e.

$$\gamma_{la}\, cos\theta + \gamma_{sl} = \gamma_{sa} \qquad (1)$$

where $\gamma_{la}$, $\gamma_{sl}$, and $\gamma_{sa}$ are liquid-air, solid-liquid, and solid-air interfacial tensions respectively.

The above equation can also be expressed as

$$cos\theta = \frac{\gamma_{sa}-\gamma_{sl}}{\gamma_{la}} \qquad (2)$$

The above equation is called as Young's equation of contact angle and is applicable to smooth surfaces [9].

$\gamma_{sl}$ in the above equation can be estimated as [10]

$$\gamma_{sl} = \gamma_{sa} + \gamma_{la} - 2\sqrt{\gamma_{sa} \times \gamma_{la}} \quad (3)$$

Surfaces with water contact angle greater than 90° are called as hydrophobic and those having water contact angle less than 90° are called as hydrophilic.

According to equations (2) and (3), a surface can be made hydrophobic by decreasing the solid-air interfacial tension. The lowest reported solid-air interfacial tension is for surfaces with trifluoro methyl (-CF3) groups (6mN/m) [11] and the corresponding water contact angle observed on such surfaces is 120°. A further increase in contact angle requires texturing of the surfaces.

### 1.1.2 Wetting on Rough Surfaces

There are two primary wetting regimes on a rough surface

1) Wenzel Regime or Homogeneous Regime

2) Cassie–Bexter Regime or Non homogeneous/composite regime

Assuming that the liquid completely wets a surface, Wenzel developed a model predicting the relation between the contact angle of a droplet on a rough surface to that on the smooth surface [12].

$$cos\theta_{rough} = rcos\theta_{flat} \quad (4)$$

Where $\theta_{rough}$ and $\theta_{flat}$ are the contact angles of the droplet on rough and flat surfaces respectively. $r$ is the roughness ratio and is defined as the ratio of surface area to the flat projected area. Now if a surface is hydrophobic to start with i.e. $\theta_{flat}$ is greater than 90°, then introducing roughness will make it more hydrophobic (since $r$ is always greater than 1). New contact angle $\theta_{rough}$ will be greater than $\theta_{flat}$. If a surface is hydrophilic to start with i.e. $\theta_{flat}$ is less than 90°, then introducing roughness will make it more hydrophilic. New contact angle $\theta_{rough}$ will be less than $\theta_{flat}$. This has been illustrated in Figure 1.2.

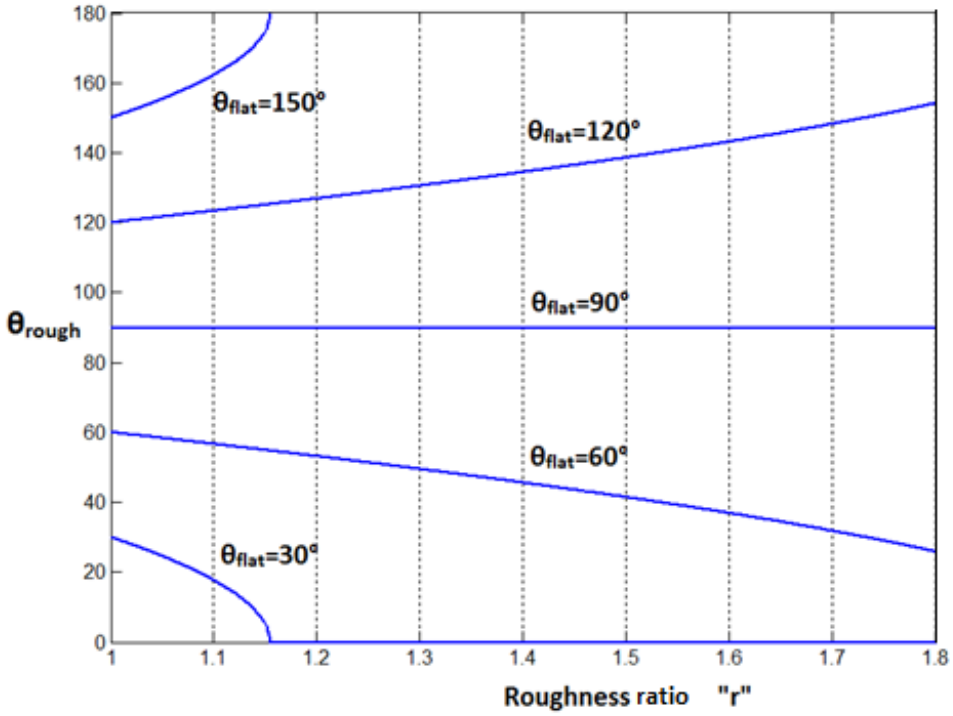


Figure 1.2 Evolution of contact angle with roughness ratio "r" for a surface [13]

The wenzel state for a droplet on a rough surface is shown in Figure 1.3.

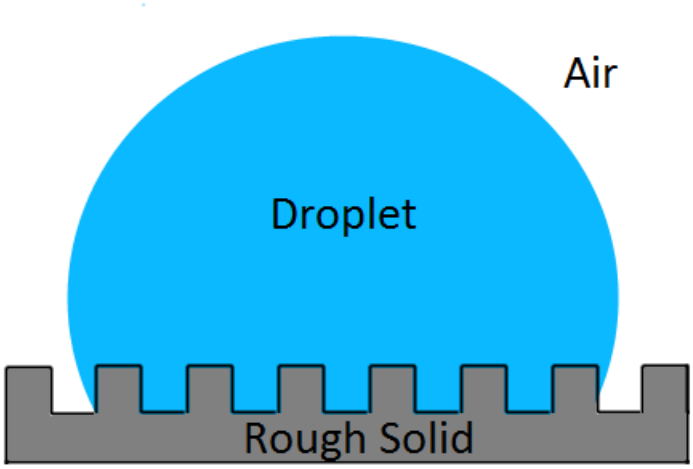


Figure 1.3 Wenzel State for a liquid droplet placed on a rough surface

The wenzel state dictates that the liquid will completely fill the texture of a solid surface. However, complete submergence of texture with the liquid becomes less energetically favorable for a hydrophobic surface. This is because the system is relatively at a higher energy when the liquid is fully wetting the texture. More stable state is attained when air pockets are formed in between the texture. Casie-Bexter extended Wenzel's work and incorporated the effect of trapped air pockets resulting in a composite solid-liquid-air interface as opposed to homogeneous solid-liquid interface [14].

$$cos\theta_{rough} = r\phi_s cos\theta_{flat} + \phi_A cos\theta_{LA} \qquad (5)$$

$\phi_s$ and $\phi_A$ being the fractional liquid-solid and liquid-air interfacial areas ($\phi_s + \phi_A = 1$). Since $cos\theta_{LA}$=180° (contact angle of water with air), entrapment of air pockets will result in an increased contact angle. Putting $cos\theta_{LA}$=180°, the above equation reduces to

$$cos\theta_{rough} = r\phi_s cos\theta_{flat} - (1 - \phi_S) \quad (6)$$

Based on eq.6, a decrease in the value of $\phi_s$ can increase the value of $\theta_{rough}$ and a surface can be made superhydrophobic (C.A greater than 150°).

The cassie-bexter state for a droplet placed on a rough surface is shown in Figure 1.4.

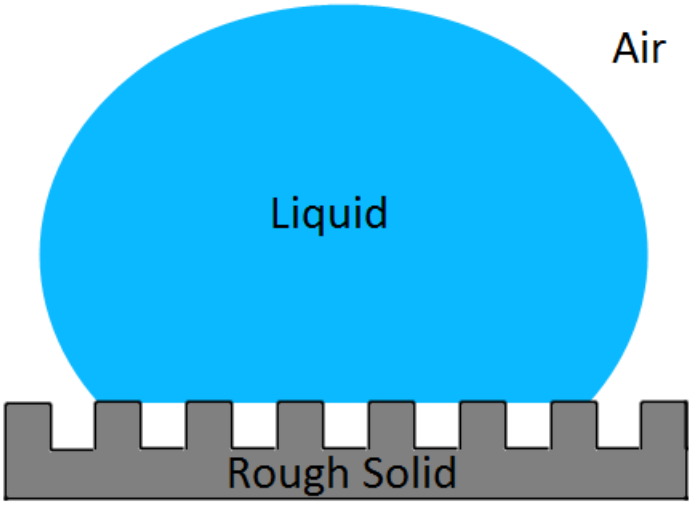


Figure 1.4 Cassie-Bexter State for a liquid droplet placed on a rough surface

Equation (6) can also be expressed in terms of $\phi_A$, where $\phi_A$ is the fractional liquid-air interfacial area.

$$cos\theta_{rough} = rcos\theta_{flat} - \phi_A(rcos\theta_{flat} + 1) \quad (7)$$

The evolution of contact angle with roughness ratio *r* and the liquid air fraction area $\phi_A$ on surfaces for which $\theta_{flat}$ is 120° and 150° has been shown in Figure 1.5.

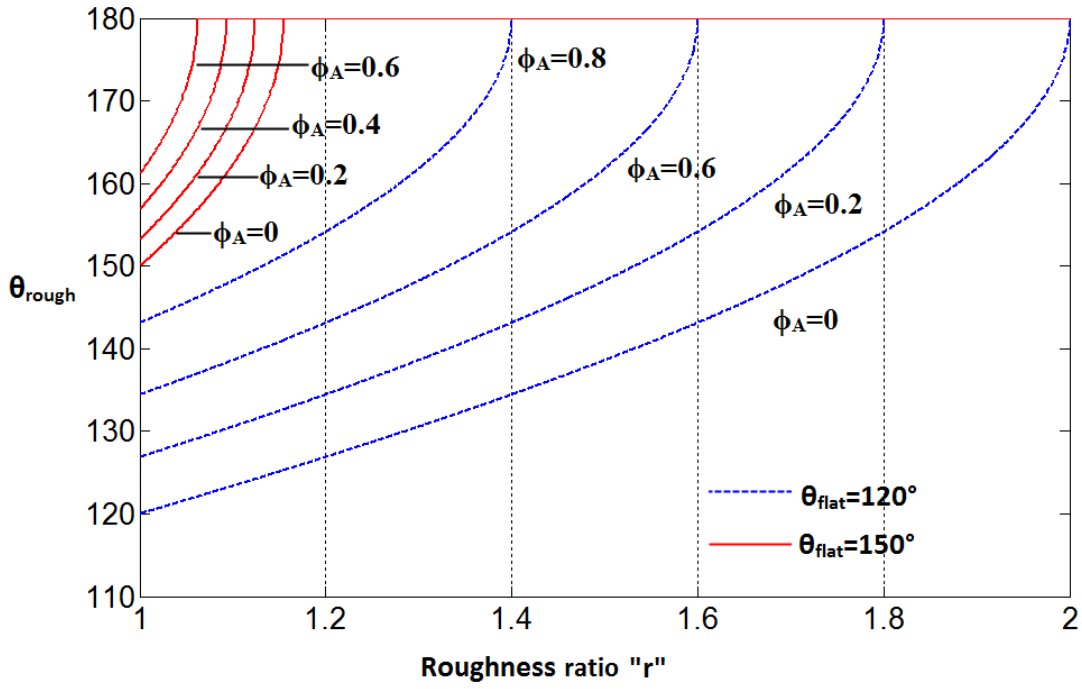


Figure 1.5 Evolution of contact angle with roughness ratio "*r*" and liquid-air fractional area $\phi_A$ for surfaces for which $\theta_{flat}$ is 120° and 150° [13]

For both of the surfaces ($\theta_{flat}$=120° and $\theta_{flat}$=150°), an increase in contact angle is brought about by an increase in both, the roughness ratio r and the liquid-air fractional area $\phi_A$.

### 1.1.3 Contact Angle Hysteresis

In general, two types of contact angle measurements are performed; static and dynamic. Static CA is measured by placing the droplet on a flat surface and then recording the value of the CA once an equilibrium is established. Dynamic contact angles are measured during the droplet growth and shrinkage. These are non-equilibrium contact angles. Dynamic CA measurement is also performed by tilting the surface and noting the values of the contact angles at the front and the back of the droplet. These contact angles are called as advancing and receding contact angles and the difference between their values is called as contact

angle hysteresis or CAH. CAH is highest just before the droplet starts sliding/rolling on the surface. CAH is a measure of how much energy is dissipated during droplet flow [15]. For surfaces with low CAH, water rolls-off at very small tilt angles and carries away dust particles along its path, giving rise to the so called self-cleaning effect [15].

Using equation (7), a relation for the contact angle hysteresis for a rough surface can be derived. The resultant equation is shown below.

$$cos\theta_{rough\ adv} - cos\theta_{rough\ rec} = r(1 - \phi_A)\left(cos\theta_{flat\ adv} - cos\theta_{flat\ rec}\right) + H_r \quad (8)$$

$\theta_{flat\ adv}$ and $\theta_{flat\ rec}$ represent the contact angle hysteresis for the smooth surface and $H_r$ represents the surface roughness effect.

The above equation can be simplified to obtain the following expression [16]

$$\theta_{rough\ adv} - \theta_{rough\ rec} = r\sqrt{1 - \phi_A}\,\frac{cos\theta_{rec\ flat} - cos\theta_{adv\ flat}}{\sqrt{2(rcos\theta_{flat} + 1)}} \quad (9)$$

For a homogeneous or wenzel interface, $\phi_A$=0.Increasing roughness ratio $r$ for such a case would increase contact angle hysteresis. For a composite or cassie-bexter interface, contact angle hysteresis is directly proportional to ($1$-$\phi_A$) i.e. a decrease in liquid-air fractional area will increase the contact angle hysteresis. This brings about the importance of micro air pockets in the texture which increase the contact angle and lower the contact angle hysteresis for a surface. Presence of a nano scale texture on top of a micro scale texture can also significantly increase the liquid-air fractional area and lower the contact angle hysteresis. A nano scale texture thus prevents the pinning of the droplet and allows it to roll-off at small inclination angles, thereby yielding the self-cleaning effect.

### 1.1.4 Lubricant Impregnated Surfaces

Conventional superhydrophobic surfaces rely on air pockets trapped between the texture to maximize the droplet contact angle with the surface. Such surfaces continue to exhibit non-wetting behavior as long as stable air pockets are maintained beneath the droplet [17]. These tiny air pockets, however, are unstable and collapse under conditions involving large wetting pressure, high temperature or humidity [18] [19], or when a damage occurs to the surface texture [20]. A low surface tension liquid can also sometimes displace these air pockets and penetrate the texture [21]. In all such cases, the droplet pins to the surface. The surface thus loses its self-cleaning ability.

To overcome the limitations associated with lotus leaf inspired surfaces, a new type of pitcher-plant (*Nepenthes*) inspired surfaces called SLIPS (slippery lubricant infused porous surfaces) have been reported [22]. These surfaces do not rely on trapped air pockets inside the texture to repel liquids. The texture is instead filled with a lubricant, thus providing a surface with an over-lying liquid interface that is ultra-smooth, chemically homogeneous, continuous and provides an extremely low contact angle hysteresis for a broad range of liquids [22].

## 1.2 Motivation

Surfaces with high optical transmittance find their use in wide range of applications such as in construction industry, automobile industry, opto-electronics, and energy conversion devices (PV panels). In all such applications, maintaining high optical transmittance is important for aesthetic and performance reasons. Surfaces are prone to lose their transmittance due to accumulation of air borne dust particles at the surface. Maintaining

optical clarity of the surfaces thus becomes challenging especially at large scales such as skyscraper windows and pretective covers for PV cells in solar farms. All such cases bring about the importance of optically transparent surfaces that are cost-effective to clean.

One of the promising solutions is to alter the wetting characteristics of a surface and make it superhydrophobic. Natural superhydrophobic surfaces like lotus plant leaves can remain clean since water droplets roll away at small inclination angles and take away dust particles along its path. This gives rise to the so called lotus effect or self-cleaning effect (Figure 1.6). A superhydrophobic surface thus can clean itself by using very little quantity of water in contrast to the conventional wetting surfaces.

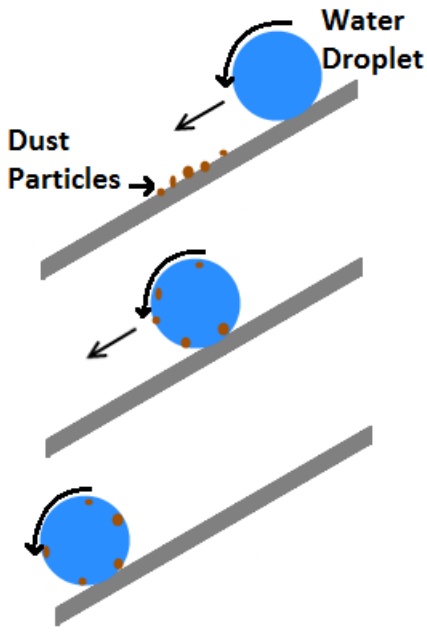


Figure 1.6 Lotus or self-cleaning effect whereby the dust particles are carried away by the rolling droplet on a superhydrophobic surface

Glass is an excellent choice of material in applications requiring high transmittance. Due to its hydrophilic nature, water droplets stick to the glass surface. These water droplets catch the dust particles and form a mud solution at the surface which greatly lowers its transmittance. This can be avoided by coating the glass surface with a superhydrophobic coating. Silica nanoparticle coating is an ideal choice because of its matching refractive index with glass which greatly improves the optical transmittance of the coating. Silica nanoparticle based coatings also possess good scratch and wear resistant properties [23]. Another facile approach to obtain optically transparent superhydrophobic coatings is to replicate textured surfaces having superhydrophobic characteristics. PDMS (Polydimethylsiloxane), a silicon-based organic polymer, is an ideal choice because of its high transparency, hydrophobic nature, and the ability to copy sub-micron features during the replication process. Filling the texture of a superhydrophobic surface with some lubricant oil can overcome many limitations associated with conventional superhydrophobic surfaces. A lubricant oil provides a smooth and homogeneous interface that can repel variety of fluids, give very low contact angle hysteresis and improve the optical transparency of the coatings [22] [24].

## 1.3 Scope of Work and Approach

The development of superhydrophobic surfaces is a multi-step process and usually involves with expensive and hazardous chemicals, longer processing times, and skilled man power. One of the facile and cost effective techniques to obtain surfaces with excellent non-wetting properties is to replicate the texture of a superhydrophobic surface using polydimethylsiloxane (PDMS). In this case, the textured surface can be copied and

replicated several times by PDMS without any damage to the surface. In the first part of the study, alumina tiles which exhibit superhydrophobic characteristics after texturing by laser, and silicon micro post arrays are replicated to obtain textured PDMS surfaces. Non-wetting characteristics, and transmittance of the resultant surfaces are aimed to be analyzed.

The second part of this study discusses the development of superhydrophobic surfaces by deposition of silica nanoparticles on the glass surface. Silica sol, mixed in three different sizes, are deposited onto the glass slide via dip coating to generate surface texture. The deposited silica particles are later functionalized with low energy silanes to reduce the surface energy, thus generating hydrophobic surface characteristics. One pot technique [25] for the synthesis of functionalized silica nanoparticles is also adopted and glass surfaces are deposited with a layer of silica nanoparticles. The performance of the resultant surfaces is assessed in a similar fashion.

Traditional superhydrophobic surfaces rely on the presence of air pockets created as a result of a micro-nano texture to repel droplets. However, these air pockets are unstable and can collapse under certain conditions. The air pockets can be filled with some lubricant to generate a relatively new class of surfaces called as SLIPS [22] (Slippery Lubricant Infused Porous Surfaces), also termed as Lubricant Impregnated Surfaces [26]. The superhydrophobic surfaces obtained by the procedures mentioned earlier are impregnated with some lubricant like Polydimethylsiloxane Oil. Non-wetting characteristics of the resultant surfaces are analyzed. In order for the oil film to be stable and be able to successfully shed the droplets, there has to be a certain match between the surface energies of this four phase system. The governing criterion for the stability of the lubricant film is discussed and the surface energy of the surface is tailored in line with the stability criterion.

The last part of this study deals with the characterization of dust particles associated with the local area (Dhahran, KSA). A setup is devised to collect dust over a period of two weeks and the dust particles are later characterized using analytical tools such as SEM, XRD and Micro-CT. The settlement of dust particles on oil impregnated surfaces is also investigated.

# CHAPTER 2

# LITERATURE REVIEW

This chapter provides extensive detail on recent developments related to the fabrication of superhydrophobic surfaces. First part of this chapter focuses on the literature related to the laser texturing of surfaces to generate superhydrophobic characteristics. The second part reviews the published work on PDMS replica molding technique to generate superhydrophobic characteristics. Literature related to silica nanoparticle based superhydrophobic coatings on glass surfaces will be presented afterwards. The last part will focus on recent developments in the field of textured surfaces impregnated with lubricant.

## 2.1 Laser Texturing of Surfaces

Laser surface texturing through combination of controlled melting and ablation at the surface is one of the promising techniques to achieve superhydrophobic characteristics on ceramic and polycarbonate substrates [27]. Considerable research studies were carried out to examine laser surface texturing and surface hydrophobicity. Laser texturing of a zirconia surface under nitrogen environment in the presence of TiC and $B_4C$ was studied by Yilbas et al. [28]. TiC and$B_4C$ particles were placed in a thin carbon film at the surface. The carbon film distributed the particles evenly at the surface and enhanced the absorption of the incident laser beam. The carbide particles enhanced the surface roughness without forming any cracks due to the generation of thermal stress arising from a mismatch between thermal

expansion co-efficient. The laser textured surface comprised of micro/nano poles and cavities and showed hydrophobic characteristics with an average contact angle of 130°.

Laser ablation of rare-earth oxide ceramics towards achieving superhydrophobic characteristics was carried out by Azimi et al. [29]. A hierarchal texture consisting of micro and nano structures was obtained after laser texturing. The texture consisted of micron sized mud-crack like features covered with nano sized protrusions. The surface showed exceptional water repellency causing the impinging water droplets to bounced off.

Triantafyllidis and Stott [30] studied surface treatment of alumina-based ceramics with the use of combined laser sources. They demonstrated that the use of combined laser sources altered the cooling rates thus avoiding the buildup of large thermal stresses. This resulted in a crack free laser treated surface. Surfaces treated with a single laser beam on the other hand showed solidification cracking.

Laser gas assisted nitriding of alumina surfaces was studied by Yilbas et al. [31].They showed that the depth of laser treated zone extended almost 40μm below the surface and composed of two regions. The first region was dense and composes of $\alpha$-$Al_2O_3$ and AlN. In the second region, randomly stacked lamellae structure was observed. The laser treated surface showed uniform features, provided that some locally scattered sub-micron cracks were observed.

In another study, laser texturing of alumina tiles under high pressure nitrogen environment was carried out by Yilbas et al. [32] to enhance the surface hydrophobicity. Laser texturing resulted in the formation of fine sized micro and nano textures at the surface. The surface energy was also modified due to the formation of AlN and AlON at the surface. Two

different states, wenzel state and cassie-bexter state, existed on the surface depending upon the surface roughness.

Laser micro-machining of thin alumina sheets was introduced as a one step process to generate superhydrophobic characteristics by Jagdheesh [33]. The effect of laser processing parameter (pulses per unit area) on the change in surface morphology and chemistry was studied. It was shown that changes in morphology influence the wetting properties more than chemical changes at the surface.

Laser surface texturing of 304S15 stainless steel to develop superhydrophobic characteristics was investigated by Ta et al. [34]. Instead of common pico\femto second laser systems employed for texturing, compact and cost-effective nanosecond fiber laser system was used. Surfaces showed hydrophilic characteristics immediately after laser irradiation. When placed in ambient air for over a period of 13 days, surfaces began to demonstrate superhydrophobic characteristics. Optimized laser processing parameters gave a water contact angle of 154° and a contact angle hysteresis of 4°.

Laser patterning of copper and brass surfaces using infrared nano second laser for enhancing surface hydrophobicity was studied by Ta et al. [35]. Wetting characteristics of laser irradiated surfaces changed from hydrophilic to superhydrophobic with time. This was associated with the partial de-oxidation of the oxides formed as a result of laser irradiation. Surfaces showed superhydrophobic characteristics with small tilt angles after an extended period of time (around 11 days). Laser irradiated copper and brass surfaces also demonstrated self-cleaning ability. These surfaces also showed the potential to be used as sensors in chemical sensing applications.

## 2.2 PDMS Replica Molding

Studies related to polydimethylsiloxane (PDMS) based hydrophobic surfaces gained considerable attention in recent years. PDMS is optically clear, inert, non-toxic, and it has non-flammable characteristics. In addition, PDMS in liquid form has superior rheological properties, which is suitable for copying and reproducing fine sized features.

Research into replica molding using PDMS gained considerable attention in recent years [36] [37] [38] . Shao et al. [36] successfully replicated different micro patterns with very high aspect ratios using PDMS replica molding technique. The challenging part was the release of the PDMS from the mold. In order to facilitate the release of negative PDMS replica from the SU-8 master mold, the master mold was first treated with Hexamethyldisilazane(HMDS) vapor. Similarly, the PDMS negative mold was treated with 1H, 1H, 2H, 2H-perfluorodecyltrichlorosilane (PFDTS) vapor in order to ease the release of replicated PDMS from negative PDMS mold.

Preventing PDMS-PDMS bonding is a major challenge in replica molding process. By coating the negative PDMS mold with hydroxypropylmethylcellulose, a hydrophilic polymer, Yang et al. [37] and Gitlin et al. [38] were successfully able to replicate different micro structures by PDMS replica molding process.

Yeo et al. [39] used PDMS double casting technique to replicate micro-patterned silicon SU-8 master molds. Micro patterns with circular, triangular, and cross shapes were successfully replicated and the wettability of the resultant surfaces was analyzed. The experimental water contact angles matched with the theoretical wenzel and cassie-bexter contact angles. It was also found out that surfaces with higher aspect ratio enhanced the

hydrophobicity of the surfaces owing to the increased surfaces roughness and formation of large air pockets beneath the water droplet.

Adithyavairavan and Subbiah [40] replicated the lotus leaf micro structures using two step polymer casting technique. By using three different polymers, Vinyl polysiloxane (VPS), polydimethylsiloxane (PDMS) and polymethylmethacrylate (PMMA), a total of six Negative-Positive mold combinations were studied. The lotus leaf replicate obtained from the VPS–PMMA mold, the texture geometric parameters such as peak height, peak width and the inter spacing between the peaks were closest to that of the actual lotus leaf. The contact angle measured for VPS-PMMS replicate was 132.1° while that of the actual lotus leaf was 152°. The reason for the difference between the contact angles was attributed to the absence of hydrophobic wax that not only covers the lotus leaf microstructure but gives it a nano texture as well.

A thermal imprint technique for preparation of superhydrophobic polymer coatings was introduced by Lin et al. [41]. A mold was first prepared by casting PDMS over the sand papers. The prepared PDMS molds were superhydrophobic and showed contact angles as high as 170°. The pattern of the PDMS molds was then transferred to the commercial polymer coatings using thermal imprint method. The non-wetting characteristics of the polymer coatings were enhanced and water contact angles of around 150° were observed. The water droplets, however, stuck to the surface due to the presence of large features protruding from the surface.

Laser irradiation of PDMS to generate superhydrophobic characteristics was studied by Yoon et al. [42]. PDMS surfaces, irradiated by a femtosecond layer, showed a water contact angle of 170° and a sliding angle of 2°. Superior superhydrophobic characteristics of the

laser irradiated surface were associated with the presence of micro and nano structures, very similar to the ones observed in lotus leaf. The negative PDMS replica of the laser treated surface had a smaller contact angle with very large hysteresis. This was due to the absence of the micro and nano size features that are emerging from the surface for laser treated surface. This caused the water droplets to be in contact in wenzel state rather than in cassie-bexter state. The positive PDMS replica, on the other hand, had a high water contact angle (150°) and small sliding angles, similar to that of laser treated surface.

## 2.3 Silica Nanoparticle Film

Silica nanoparticles have been extensively used to give wetting/non-wetting characteristics to a variety of substrates. By functionalizing the nanoparticles with appropriate functional groups, superhydrophilic / superhydrophobic or omniphilic / omniphobic surfaces could be realized.

Stober et al. [43] pioneered the technique for the synthesis of spherical silica nanoparticles using TEOS (tetraethyl orthosilicate), ammonium hydroxide, ethanol and water. The effect of concentration of TEOS, water and ammonium hydroxide on the mass fraction and final particle size has been extensively studied [44] [45] [46].One of the interesting properties of silica nanoparticles is that its surface can easily be functionalized with some desired functional group. Suratwala et al. [47] modified the surface of silica sols by reaction with HMDS(hexamethyldisilazane) and ETMS (ethoxytrimethylsilane) to produce hydrophobic trimethylsily functionalized silica nanoparticles. The percentage of functionalization varied between 5% - 33% and was strongly dependent upon the starting nanoparticles chemistry, HMDS concentration, and reaction time.

Yong et al. [25] used one pot technique to prepare spherical mono dispersed functionalized silica nanoparticles directly from TEOS. The surfaces of silica nanoparticles were modified and made hydrophobic by reaction with organosilanes such as APTMS (3-aminopropyltrimethoxysilane), ITMS (3-isobutyltrimethoxysilane) and (OTES) octyltriethoxysilane. All the chemicals, including the modifier silane were mixed in one pot to obtain octyl-, minopropyl-, and isobutyl- functionalized silica nanoparticles.

By using a layer by layer technique, Bravo et al. [48] fabricated a multilayered silica nanoparticle superhydrophobic film on glass. The glass slides were dipped repeatedly in different solutions to create an adhesion layer, followed by the body and the top layer. A hierarchal texture was created by using 50nm and 20nm silica nanoparticles in the body layer and 20nm particles in the top layer. The number of layers were optimized for the highest optical transmittance (around 90%) and maximum WCA (161°). The procedure adopted was very tedious and involved a lot of chemicals.

Ling et al. [49] employed a simple dip coating technique to obtain a silica nanoparticle coating on the glass slide. Prior to dip coating, an amine terminated self-assembled monolayer was grown on the surface of glass. It enabled the silica nanoparticles to leave large gaps in between while forming a coating at the glass surface. Static WCA of 152° was observed after treatment with PFOTS. The CAH, however, was relatively higher, averaging around 25°. The UV/Vis spectrum showed a slight decrease in transmittance at smaller wavelengths.

Yang Li et al. [50] fabricated a transparent superhydrophobic coating on glass by LbL (Layer by Layer) deposition of PAH (poly allylamine hydrochloride)/ SiO2 nano particle films on top of PDDA-silicate film. It was followed by calcination and CVD (chemical

vapor deposition) of fluoroalkylsilane. A total of four cycles of PAH/$SiO_2$ deposition yielded a static WCA of 157°.

By using spray coating technique, Ogihara et al. [51] formed a hydrophobic silica nanoparticle coating on the glass surface. Functionalized silica nanoparticles suspended in propanol were used for the coating purposes. The obtained coating consisted of very fine micro and nano structures and yielded a high optical transparency. The effect of surface treatment of the glass on the hydrophobic characteristics of the resultant surfaces was also investigated. For the untreated glass surfaces, the silica nanoparticle films didn't show superhydrophobic characteristics. This was due to the high surface energy of the glass surfaces which caused the water droplets to stick to it. For the glass surfaces treated with fluorine groups, formation of a uniform silica nanoparticle film was difficult because of the poor wettability of the glass. Glass surfaces treated with dodecyl groups were most suited for forming a transparent superhydrophobic silica nanoparticle film.

## 2.4 Lubricant Impregnated Surfaces

Filling the texture of a superhydrophobic surface with some lubricant oil is a relatively new concept and such surfaces have gained quite an attention in recent years [22] [52] [53]. Traditional superhydrophobic surfaces rely on the presence of air pockets to repel the droplets. The air pockets, however, are unstable and a water droplet can easily penetrate the texture and be in the wenzel state. This situation is avoided in lubricant infused surfaces by selecting a lubricant oil that completely fills the texture and provides an interface that is smooth and chemically homogeneous. Lubricant infused surfaces, however, become more complex due to the introduction of an additional phase and such a system has far

more possible thermodynamic states which may exist when a droplet is placed on such surfaces. Smith et al. [26] investigated these states and the criterion under which one thermodynamic state may be more favorable . It was shown that a total of twelve different thermodynamic states are possible in these complex 4 phase systems. It is desirable for lubricant impregnated surfaces to have a stable lubricant film beneath as well as outside the droplet. Such thermodynamic state is possible if the following two conditions are satisfied; $\theta_{os(a)}$=0 and $\theta_{os(w)}$=0 i.e. the contact angle of oil(o) on solid(s) in the presence of air(a) and water(w) is zero. In case of a non-zero contact angle, complete encapsulation of texture by the lubricant ceases to occur. A critical contact angle based on the texture parameters has been defined as

$$\theta_c = cos^{-1}\frac{1-\phi}{r-\phi}$$

where "r" is the roughness ratio and ϕ is the projected area of the surface occupied by the solid. A surface for which $0 < \theta_{os(a)} < \theta_c$, the fractional area of the surface, as defined by ϕ, will not be covered by thin lubricant film. It will instead be exposed to air/vapor phase. Surfaces for which $\theta_{os(a)} > \theta_c$, the liquid will displace the lubricant and get impaled by the texture. Similar arguments can be made when $0 < \theta_{os(w)} < \theta_c$. The surfaces features, as defined by ϕ, will not be covered by lubricant but rather by the liquid. When $\theta_{os(w)} > \theta_c$, the liquid displaces the lubricant and completely wets the texture as in wenzel state.

Kim et al. [54] investigated the effect of surface roughness on lubricant loss under high shear conditions and found out that nano structured surfaces were best at retaining a thin layer of lubricant because of the capillary forces. It was also concluded that two tiered roughness was not necessary and that a single level of roughness was sufficient enough to

hold the lubricant in place. Smith et al. [26] ,however, reported that the presence of a nanostructure on top of a microstructure significantly reduced water droplet pinning for surfaces for which the emergent texture features were not covered by a lubricant film.

Anand et al. [55] studied droplet condensation on lubricant impregnated surfaces and found out that the droplets stayed mobile and didn't pin to the substrate. Surfaces for which the lubricant was not fully encapsulating the texture, a nano texture allowed the droplets to move with significant velocities. This provided fresh nucleation sites for the vapors to condense, grow and subsequently be removed from the surface. In case of conventional superhydrophobic surfaces, nucleation of droplet starts within the texture itself. The droplet is thus impaled by the texture and does not stay mobile.

Kim et al. [56] demonstrated that lubricant infused surfaces can be used as ice-repellent coatings because of their enhanced condensate removal abilities. Aluminum was used for study because of its wide applicability in transportation and construction industry. After forming a texture on aluminum surface, it was infused with a lubricant. They demonstrated that the lubricant infused aluminum surfaces resisted ice-formation at sub-zero temperatures. In this case, the condensating water droplets stayed mobile and didn't pin to the surface. Such surfaces also showed very low ice-adhesion and allowed its easy removal once formed at the surface.

## 2.5 Proposed Work in Light of Literature

Superhydrophobic surfaces with high optical transmittance have gained considerable attention in recent years due to their ability to provide self-cleaning characteristics [2]-[4] .

These surfaces can be used for the applications where high optical clarity becomes crucial such as PV-Panels protection covers. Although several studies have been carried out to produce surfaces with superhydrophobic characteristics and high optical transmittance[36]-[56], the task of devising cost-effective techniques that are commercially scalable for large area production of optically transparent superhydrophobic surfaces still needs to be addressed. Laser texturing is one of the processes to generate a fine texture at the surfaces for enhancing the hydrophobic characteristics. This process, however, has limitations in terms of being expensive and requiring qualified manpower. In addition, the process does not suit for the commercial production of large area superhydrophobic surfaces. The texture of a laser irradiated surface, however, can be replicated by using Polydimethylsiloxane (PDMS) that is transparent, inexpensive, and has ability to copy sub-micron features. PDMS replication process is fast and simple and can be repeated several times to obtain superhydrophobic surfaces. Replication of textured surfaces by PDMS is, thus, introduced as a facile and cost-effective approach to obtain superhydrophobic surfaces. Another facile approach for generating superhydrophobic characteristics on surfaces is by the introduction of silica nanoparticles via deposition processes. A fine layer of silica nanoparticles can aid to generate a lotus effect without compromising the optical transmittance of the surfaces. Another emerging class of surfaces that provide near to zero contact angle hysteresis for the droplets with extremely high optical transmittance are lubricant impregnated surfaces. In the present study, a facile and simple technique for the preparation of the lubricant impregnated surfaces is to be formulated. In this case, Glass wafers can be used as the substrate material and silicone oil can be incorporated as a lubricant.

# CHAPTER 3

# EXPERIMENTAL WORK

This chapter covers the details of the experimental work conducted for the thesis. The characterization techniques used have also been included. First part of this chapter discusses the experimental details for texturing of the alumina tiles by laser irradiation. It is followed by the detail of the protocol adopted for the replication of the textured surfaces using Polydimethylsiloxane (PDMS). Synthesis of hydrophobic silica nanoparticles by one pot technique is then discussed. The details of the coating methods employed, dip coating and solvent deposition, for coating the glass surface with silica nanoparticles are then discussed. The procedure adopted for impregnation of the textured surfaces with lubricant is introduced afterwards.

## 3.1 Laser Texturing of Alumina Surfaces

Alumina ($Al_2O_3$) tiles with 3 mm thickness were purchased from Ceram Tec-ETEC. The surface of the workpieces was irradiated with the $CO_2$ laser (LC-ALPHAIII with wavelength 10.6 µm). Laser spot diameter at the irradiated surface was about 200 µm while the nominal output power of the laser was 2 kW. Nitrogen gas jet at high pressures was also used during the laser irradiation of the surfaces. The pulsing frequency of the laser was adjusted at 1500 Hz which gave rise to 68% overlapping ratio for the consecutive irradiated spots. Laser power, beam intensity distribution, spot size, scanning speed, and pulse repetition rate were the variables which influenced the laser treated surface properties.

By controlling these parameters, crack free texture was obtained. Laser treatment conditions are given in Table 3.1

Table 3.1 Laser processing parameters

| Feed Rate (m/s) | Power (W) | Frequency (Hz) | Nozzle Gap (mm) | Nozzle Diameter (mm) | Focus Diameter (mm) | $N_2$ Pressure (kPa) |
|---|---|---|---|---|---|---|
| 0.1 | 2000 | 1500 | 1.5 | 1.5 | 0.3 | 600 |

## 3.2 Silicon Micro-Post Arrays

Square Micro Post Arrays with side length "*a*" of 10µm were etched on a silicon wafer using standard photo-lithography procedure. Three different samples were prepared with edge to edge post spacing "b" of 10, 25 and 50 µm while post height "*h*" was kept constant at 10µm. The texture dimensions have been shown in the schematic in Figure 3.1.

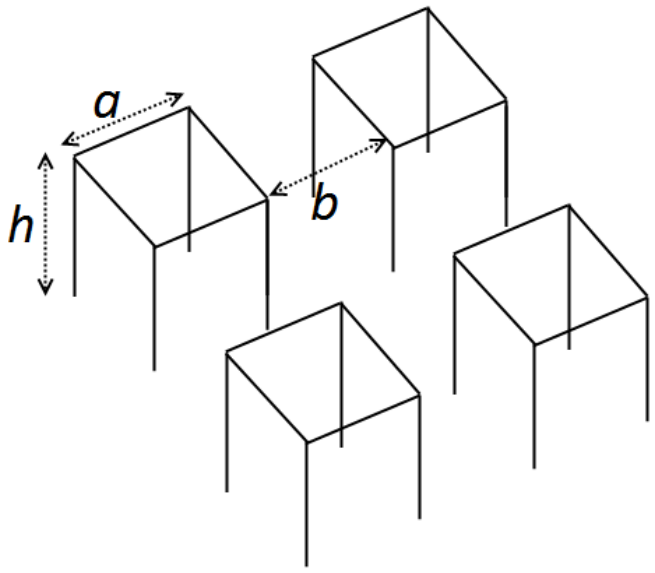


Figure 3.1 A schematic of silicon micro post array surface

## 3.3 Replication of Textured Surfaces Using PDMS

PDMS (Polydimethylsiloxane), an organic-silicon polymer, was chosen as a candidate material for replication studies. PDMS is optically clear, inert, non-toxic, and has non-flammable characteristics. In addition, PDMS in liquid phase easily wets the textured substrate and is thus able to copy the sub-micron features as well [38]. PDMS also has a low surface energy which allows its easy removal from the surface being copied. PDMS used in this study was purchased from Dow Corning, USA (sold under the brand name of Sylgard 184). It comes in two parts; elastomer base and hardening agent. In all of the studies, the base and the hardening agent were mixed in a weight ratio of 10:1. After thorough mixing, the mixture was degassed by putting in a vacuum desiccator at 74 cm Hg vacuum for 30 minutes. The mixture was then poured over the surface to be copied. It was then kept in an oven at 150°C for 30 minutes. The solidified PDMS was then carefully peeled off with the help of tweezers. To obtain the exact replica of the surface, PDMS was prepared again using the same procedure, poured over the copied PDMS, cured in the oven and then peeled off slowly. To allow for the easy removal of PDMS, the surface to be copied is often covered with low energy silane. The procedure to obtain replicated PDMS surfaces has been graphically shown in the Figure 3.2.

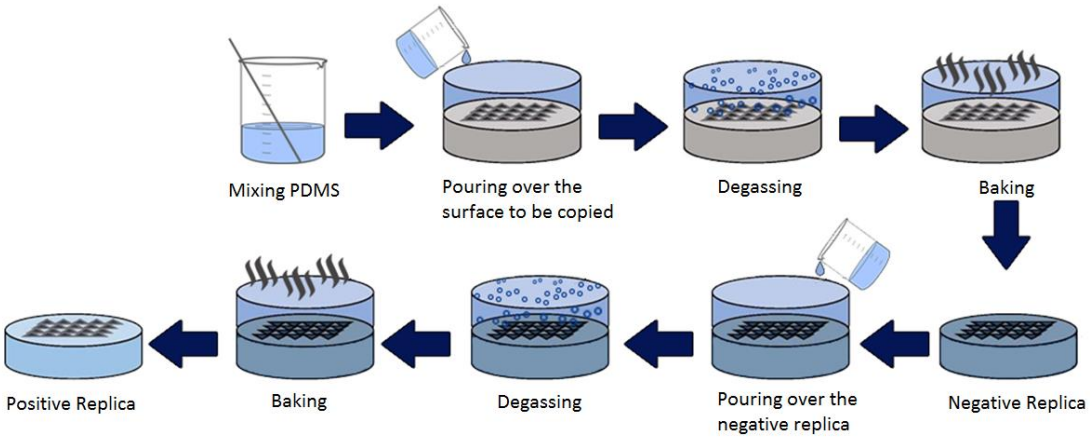


Figure 3.2 A schematic view of a protocol to replicate a textured surface by PDMS

## 3.4 Functionalization of Surfaces

In order to reduce the free energy of surfaces, they are often functionalized with some low energy silanes. In our study, two silanes were used for the aforementioned purpose; Octadecyltrichlorosilane (OTS) and Trichloro(1H,1H,2H,2H-perfluorooctyl) (PFOTS). Octadecyltrichlorosilane in our study was deposited by solution immersion. 3 drops (roughly 0.075ml) of OTS were put in 10ml of Hexane and the substrate was kept in that solution for 4 hours. After cleaning with acetone, ethanol and then acetone again, the substrate was then baked in an oven at 115°C for 15 min. Trichloro(1H,1H,2H,2H-perfluorooctyl) in our study was deposited via vapor deposition. Few drops of PFOTS were put on a glass slide in a vacuum desiccator along-with the surfaces to be treated. The system was kept at a vacuum of about 74cm Hg for 4 hours after which the samples were removed and baked in an oven at 115°C for 15 min.

## 3.5 Synthesis of Functionalized Silica Nanoparticles

One pot technique for the synthesis of functionalized silica nano particles was adopted from the work of Yong et al. [25]. Tetraethyl orthosilicate (TEOS), isobutyltrimethoxysilane (OTES), ethanol, and ammonium hydroxide were used in the synthesis. In this case, 14.4 mL of ethanol, 1 mL of ultrapure water, and 25 mL of ammonium hydroxide were mixed and stirred for 12 min. 1 mL of TEOS, diluted with 4 mL of ethanol, was then added to the mixture. After 30 minutes, 0.5 mL of TEOS diluted in 4 mL ethanol was added. After 5 min, the modifier silane molecule (OTES) was added in a molar ratio of 3:4 with respect to the second addition of TEOS. The final mixture was stirred for 20 h at room temperature and later centrifuged and washed with ethanol for removal of reactants.

## 3.6 Solvent Deposition of Functionalized Silica Nanoparticles

The functionalized silica nano particles obtained were re-dispersed in iso-propyl alcohol at a concentration of 15mg/ml. The solution was then put on the surfaces kept horizontally at a concentration of 0.1ml/$cm^2$ for PDMS and 0.25ml/$cm^2$ for glass surfaces. The solution was then allowed to evaporate at room conditions.

## 3.7 Dip Coating in Silica Nanoparticles

The glass slides were first cleaned by a soap solution to remove grease and dirt. Piranha solution was prepared by mixing $H_2SO_4$ and 33% $H_2O_2$ in 5:1 volume ratio and the glass slides were immersed in that solution for 30 minutes. After rinsing thoroughly with DI water, the glass slides were sonicated in ethanol, acetone and then ethanol again, followed

by a final rinse in DI water. The glass slides were then dried under Nitrogen gas and used immediately to avoid contaminants buildup. Suspension of colloidal silica particles in three different sizes (220 nm, 75nm and 30 nm) in DI water were obtained from FUSO Chemicals, Japan. These were mixed in equal volumes and then ethanol was added to the mixture to achieve a volume ratio of 15:1 (ethanol to colloidal silica mixture). The mixture was sonicated for 15 minutes to obtain a homogeneous distribution of particles. Glass slides, cleaned using the same procedure as mentioned before, were immersed into this colloidal silica mixture for 5s. They were then withdrawn vertically with a velocity of 150 µm/s using MTI Dip Coater. The process has been illustrated in Figure 3.3.The silica-coated glass slides were then baked in an oven at 200C for 2 hours to dry out the solvent and then air cooled.

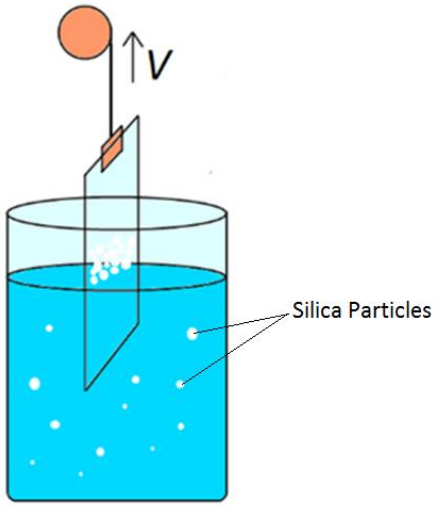


Figure 3.3 Dip coating of glass surfaces in silica particles suspension

## 3.8 Oil Impregnation of Textured Surfaces

The textured surfaces were impregnated with oil by dipping them in oil bath for 1 min. They were then withdrawn vertically with very small velocity (1mm/min) so that no excess oil film remained on the surface. Figure 3.4 illustrates the process.

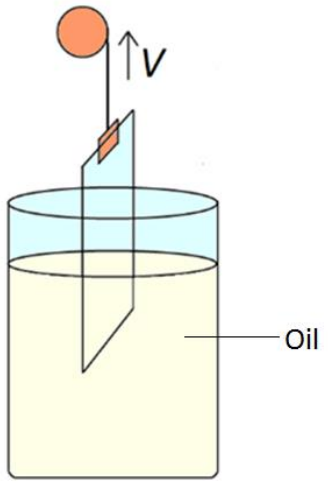


Figure 3.4 Oil/Lubricant impregnation of textured surfaces

## 3.9 Collection and Characterization of Dhahran, KSA Dust

Glass slides were placed horizontally in the open environment for a period of over two weeks in order for the dust to settle at the surface. The dust was gently removed and passed through a sieve to remove other contaminants. The dust was then characterized using different analytical tools.

## 3.10 Materials

Polydimethylsiloxane (Sylgard-184) was obtained from Dow Corning, USA. OTS (n-Octadecyltrichlorosilane) (90%) was obtained from Vesino Industrial Co., China. PFOTS

(Trichloro(1H,1H,2H,2H-perfluorooctyl) was obtained from Sigma Aldrich, USA. Silicone oil (380 mPas viscosity) was purchased from Loba Chemie, India. Acetone, Ethanol, n-hexane, $H_2SO_4$, 30%w/w $H_2O_2$, Iso-propyl alcohol, Tetraethyl orthosilicate (TEOS), isobutyltrimethoxysilane (OTES), and ammonium hydroxide were obtained from Scharlau, Spain. FUSO PL-20 (220 nm diameter silica particles) (20 wt.%), PL-7 (75 nm diameter silica particles) (23 wt%), and PL-3 (35 nm diameter silica particles) (20wt%) colloidal silica were obtained from FUSO Chemicals, Japan. Microscope Glass Slides were obtained from Fisher Scientific, USA. Milli-Q water with resistivity greater than 18.2 MΩ·cm was used.

## 3.11 Analysis

SEM imaging was performed on LYRA Tescan 3 Field Emission Scanning Electron Microscope. AFM by NanoMagnetics was used in Dynamic mode to analyze the surface texture. The tip was made of silicon nitride probes (r = 20 - 60 nm) with a manufacturer specified force constant, k, of 0.12 N/m. The wetting experiment was performed using Kyowa (model - DM 501) contact angle goniometer. A sessile drop method was considered for the contact angle measurements and 7µL droplets were deposited onto the surface using an automated dispensing system. Dynamic contact angles were measured by tilting the stage and recording the values of the contact angle at the front and the back of the droplet. The instant where the droplet rolled off from the substrate was noted and the values of advancing contact angle $\theta_{adv}$ (at the front of droplet) and receding contact angle $\theta_{rec}$ (at the back) were used for calculating contact angle hysteresis ($\theta_{adv} - \theta_{rec}$). A total of five readings were taken and the standard error was calculated for each measurement. MTI-Dip Coater

allowing substrate velocities down to 1mm/min was used for coating purposes. UV-VIS Spectrophotometer (Jenway 67 series) was used to measure the transmittance of the workpieces.3d optical images of the workpieces were taken with Bruker Contour-GT Microscope. Fourier transform infrared spectroscopy (ATR-FTIR) was carried out using Bruker Vertex 70v FTIR Spectrometer. XRD measurements were carried out on Rigaku Mini Flex Benchtop XRD system with the following settings

- Voltage=50 kV
- Current=15mA
- Scan speed= 4°/min.

ASTM C1327-99 standard test method for Vickers indentation hardness was adopted to quantify the surface microhardness. Microphotonics digital microhardness tester (MP-100TC) was used for the measurement. A linear micro-scratch tester (MCTX-S/N: 01-04300) was used for friction coefficient measurements. The equipment was set at the contact load of 0.03 N and end load of 5 N. The scanning speed was 5 mm/min and loading rate was 1 N/s. The total length for the scratch tests was 0.5 mm.

X-ray photoelectron spectroscopy (XPS) measurements were performed on ESCALAB 200-X spectrometer (VG Instrument) using AlKα radiation (1,486.6 eV) from a Mg/Al anode (300W). $Ar^+$ ion current was maintained at 3 μm/cm2 during the measurement.

Skyscan 1172 Micro-CT Imaging Facility was used to obtain tomographs for the dust particles. Table 3.2 summarizes the scan conditions adopted for the analysis.

Table 3.2 Micro-CT scan conditions for dust particle

| Voltage | Current | Filter | Pixel Size | Exposure | Rotation Step | Frame Averaging | Random Movement |
|---|---|---|---|---|---|---|---|
| 59 kV | 165 µA | Al 0.5mm | 0.96 µm | 2855 ms | 0.4° | 6 | 10 |

Reconstruction of the projection images was done using *N-Recon* Software with the parameters mentioned in Table 3.3.

Table 3.3 Reconstruction parameters for dust particle in N-Recon software

| Beam Hardening Correction | Post-Alignment | Smoothing | Ring Artifact Correction | Hounsfield Units (Min) | Hounsfield Units (Max) |
|---|---|---|---|---|---|
| 0% | 5 | 0 | 6 | 610.7 | 34000 |

The projection images were analyzed with Bruker's *CT-An* and Open Source *Image J* Software. Table 3.4 highlights sequence of operations performed for the successful segmentation of the individual dust particle.

Table 3.4 Sequence of operations in Image J and CT-An software for successful segmentation of dust particle

| **Operation** | **Value** |
|---|---|
| *Image J Software* | |
| Thresholding Range | 12-255 |
| Gaussian Blurr | Radius=1 |
| Unsharp Mask | Radius=1, Mask=0.9 |
| *CT-An Software* | |
| Thresholding Range | 20-255 |
| 3d Sweep (Despeckle) | |
| Shrink-Wrap ROI | |

# CHAPTER 4

# RESULTS AND DISCUSSIONS

This chapter focuses on the surface characterization of the obtained workpieces. Analytical tools such as SEM, AFM, FTIR, 3d-optical microscope, contact angle goniometer, UV/Vis spectroscopy have been used to analyze the surface characteristics, non-wetting performance and optical transmittance.

## 4.1 Laser Texturing of Alumina

Laser texturing of alumina surface is adopted as a single step process to generate superhydrophobic characteristics at the surface. Laser treated surface consists of regular scanning tracks as shown by the 3d optical image of the surface in Figure 4.1.

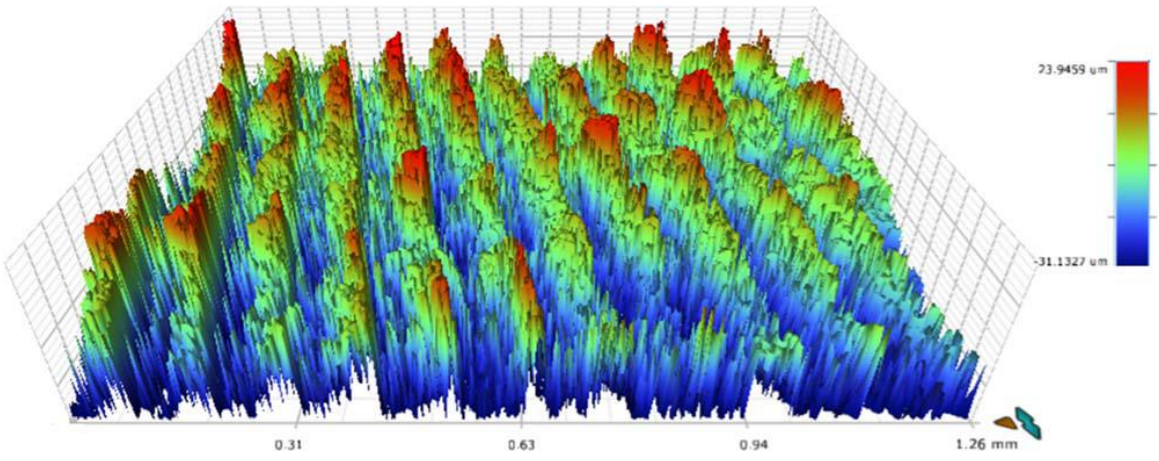


Figure 4.1 3-D optical image of laser treated alumina surface showing regular scanning tracks

Figure 4.2 shows the SEM micrographs for the laser treated alumina surface.

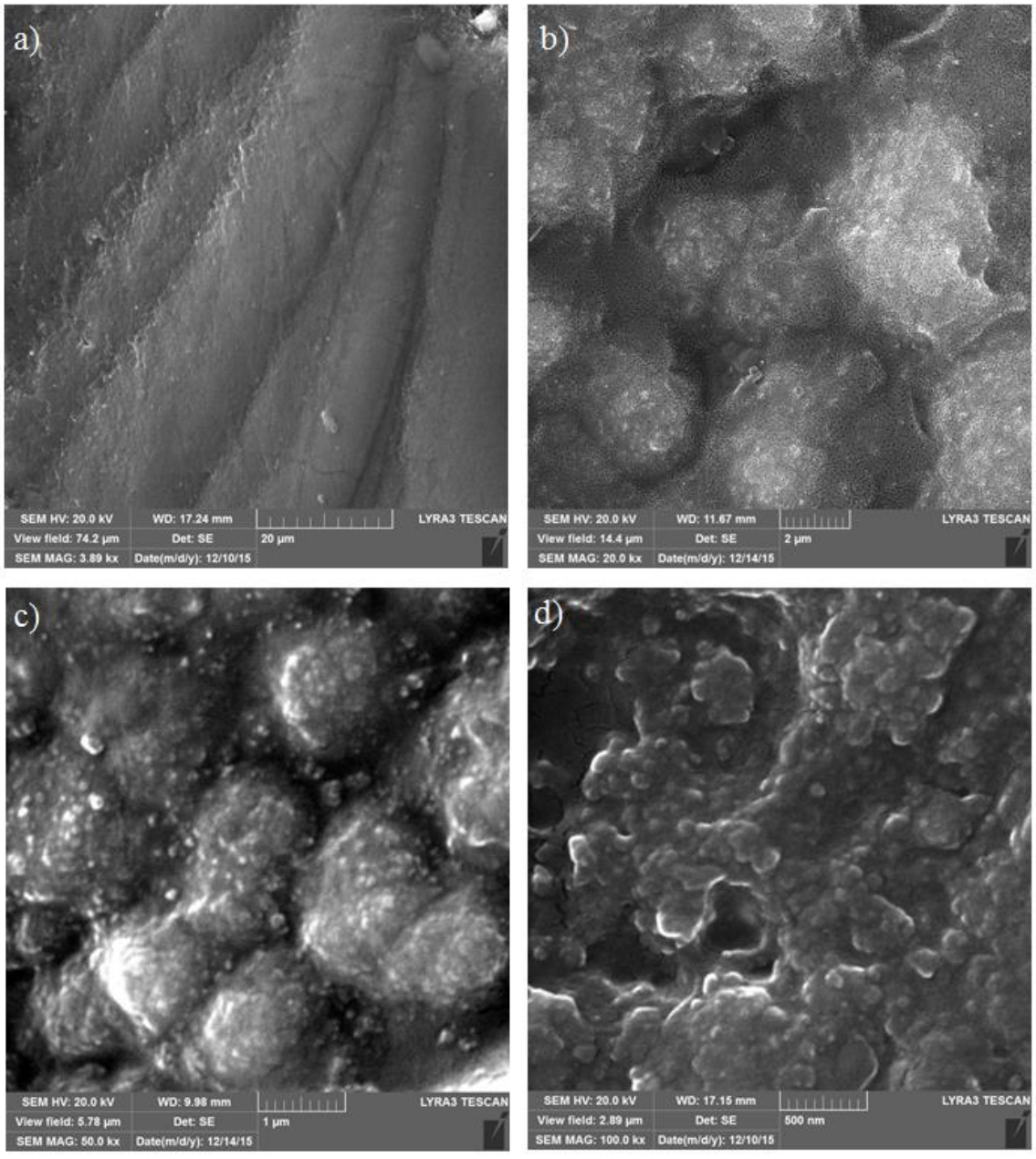


Figure 4.2 SEM micrographs of laser treated alumina surface: a) overlapping of laser irradiated spots, b) small size pillars and cavities, c) hierarchical surface texture, and d) nano size pillars in hierarchical texture

Since laser repetitive pulses with 1500 Hz frequency is used to irradiate alumina surfaces, overlapping of irradiated spots form regular ablation/melting tracks at the surface along the laser scanning direction (Figure 4.2(a)). Overlapping ratio of irradiated spots is in the order of 68%. Moreover, combination of ablation and melting gives rise to formation of small cavities and poles at the laser irradiated surface (Figure 4.2(b)). Although the distribution of poles demonstrates a non-uniform behavior, some degree of a hierarchical texture is formed at the surface (Figure 4.2(c)) and (Figure 4.2(d)). In addition, the pole height varies within 2.6 μm, which can be observed from Figure 4.3, in which atomic force microscope (AFM) image is shown (Figure 4.3(a)) together with the surface texture profile along a line scanned (Figure 4.3(b)). The surface roughness of the laser treated surface is in the order of 0.82 μm. It is evident from AFM image that the surface consists of fine sized poles and cavities.

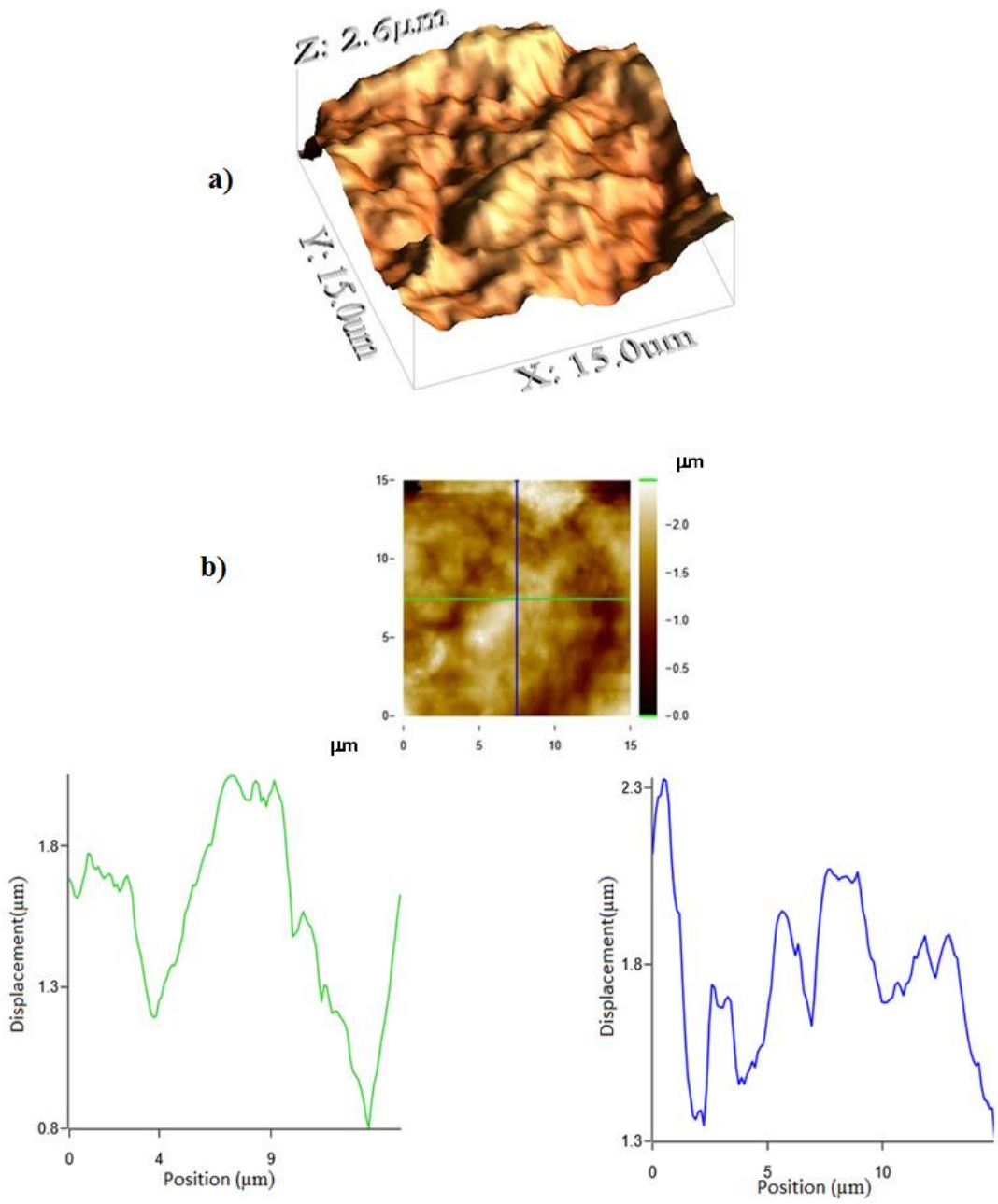


Figure 4.3 Atomic force microscope image and line scan at laser treated alumina surface: a) 3-D image of surface, and b) line scans at the surface

Since laser beam intensity distribution is Gaussian across the irradiated spot, laser beam intensity remains high at the irradiated spot center. This gives rise to a local evaporation at the surface while melting takes place at the edges of the irradiated spot. The melt flows from the irradiated spot edge towards the cavity center modifying the cavity size and texture at the irradiated surface. The flow of melt from the neighboring irradiated spot towards the previously formed spot, due to consecutive pulses, further modifies the surface texture, which in turn gives rise to a hierarchical topography of the surface. A close examination of the surface reveals that no micro-crack and large size void is formed at the surface (Figure 4.2(b)). This is attributed to the self-annealing effect generated during the repetitive pulse heating of the surface [57]. In this case, heat conduction from the recently formed irradiated spot towards the previously formed spot alters the cooling rates below the heated surface. This in turn reduces the thermal stress in the surface vicinity. Figure 4.4 shows SEM micrograph of the cross-section of laser treated layer.

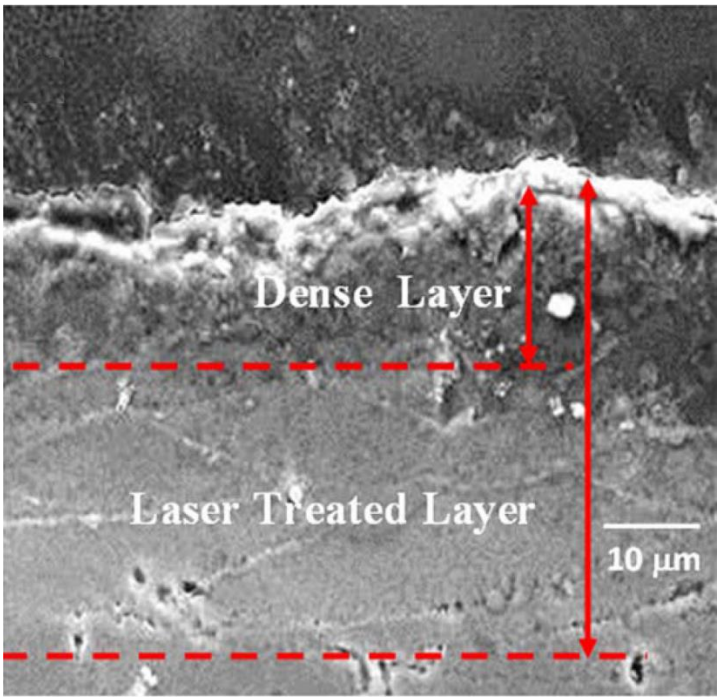


Figure 4.4 SEM micrograph of cross-section of laser treated alumina surface

The depth of laser treated layer extends almost 40 μm below the surface. The top zone consists of a dense layer in which fine size grains are formed. The formation of a dense layer is attributed to the high cooling rates and generation of nitride compounds at the surface region.

Since nitrogen at high pressure is used as an assisting gas during laser texturing of alumina surfaces, nitride compound (AlN) is formed at the surface. The formation of AlN is evident from the X-ray diffractogram of the surface as shown in Figure 4.5.

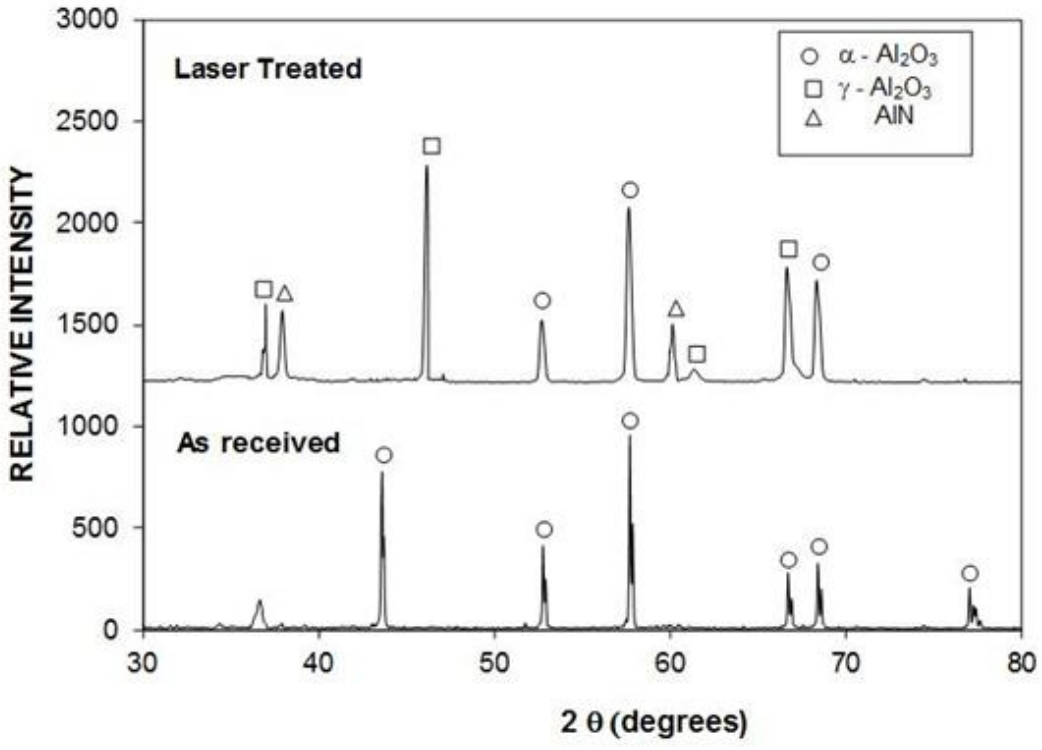


Figure 4.5 X-ray diffractogram of laser treated and as received alumina workpieces.

XRD diffractogram of laser treated alumina reveals the presence of AlN. AlN formation can be attributed to the following reactions: alumina oxide ($Al_2O$) and carbon monoxide (CO) are formed through the following reaction at the treated surface $Al_2O_3 + 2C \rightarrow Al_2O+2CO$. AlN is then formed through the reaction under high pressure nitrogen environment [58]: $Al_2O + CO + N_2 \rightarrow 2AlN + CO_2$. Energy dispersive spectroscopy (EDS) analysis for the laser treated surface is carried out to assess the elemental changes. The elemental composition of the laser-treated surface is given in Table 4.1.

Table 4.1 EDS results in the surface region of the laser treated alumina

| Spectrum | **N** | **O** | **Al** | 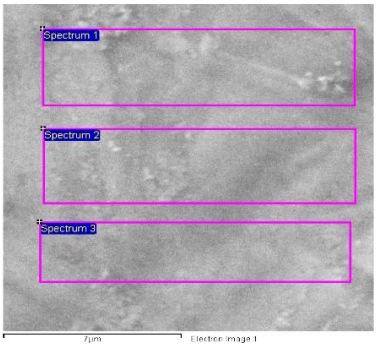 |
|---|---|---|---|---|
| Spectrum 1 | 4.7 | 40.6 | Balance | |
| Spectrum 2 | 5.1 | 43.4 | Balance | |
| Spectrum 3 | 3.8 | 44.7 | Balance | |

The data reveals that the elemental composition does not alter notably at the laser treated surface. However, nitrogen presence in EDS data indicates the formation of nitride species at the surface, despite the fact that the precise quantification of nitrogen is difficult in the EDS system because of being a light element. To confirm the presence of AlN at the laser treated surface, XPS measurements were carried out. The XPS spectral lines for AlN, as shown in Figure 4.6, reveal the presence of Al and N peaks. The Al 2p line is centered at 74.3 eV (Figure 4.6 (a)) and N 1s line at 399 eV (Figure 4.6 (b)). These lines are in similar position to those shown in the literature [59].Consequently, AlN compound is formed during the laser processing of the surface.

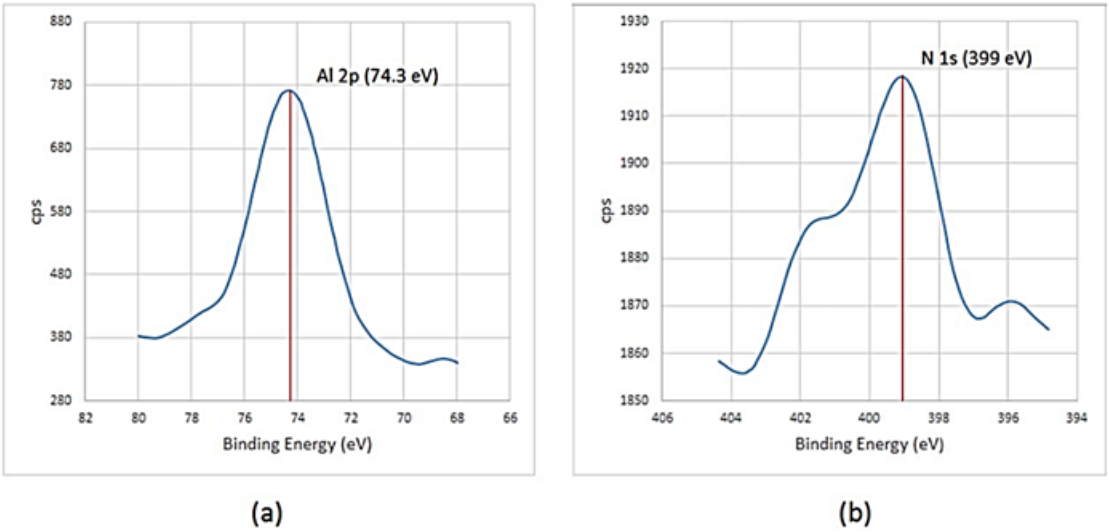


Figure 4.6 XPS Spectral Lines for AlN in laser treated alumina: (a) Aluminum 2p line and (b) Nitrogen 1s line

The surface free energy of laser treated alumina surface was measured using the sessile droplet technique. Water, Glycerol, and Diiodomethane were used as test liquids. The surface energy formulation incorporating the contact angle measurement technique has been presented in the earlier study [60]. The surface energy measured was in the order of 51.6±4 mJ/m$^2$.

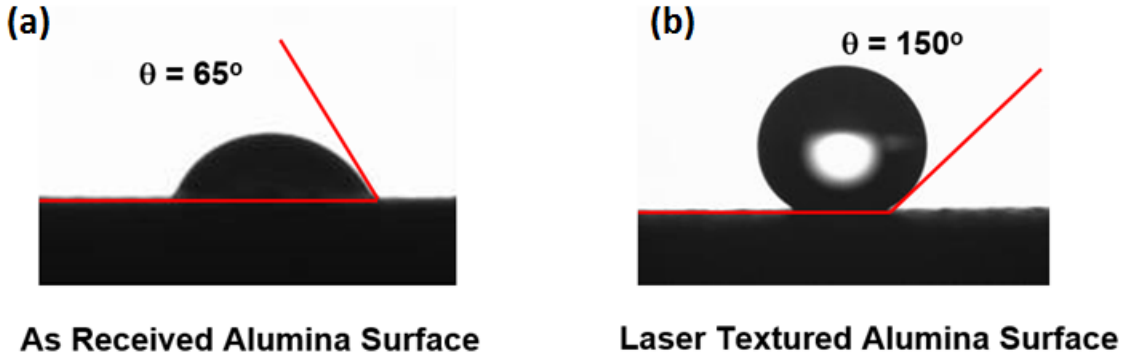


Figure 4.7 Contact angle of water droplet on (a) as received alumina surface, (b) laser treated alumina surface.

Figure 4.7 shows water droplet images obtained for as received alumina surface (Figure 4.7(a)) and laser textured surface (Figure 4.7(b)). Formation of low surface energy AlN compounds and micro/nano textures at the surface resulted in high contact angle of the droplets.

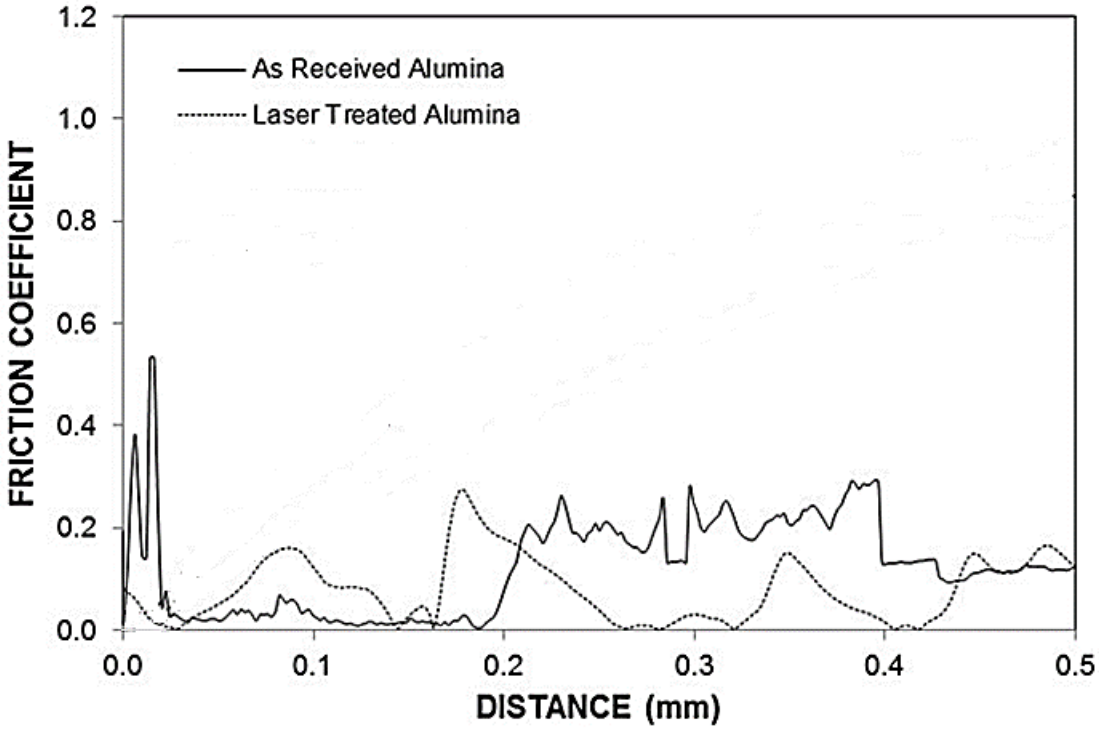


Figure 4.8 Friction coefficient for as received alumina surface and laser treated alumina surface

The friction co-efficient for the laser treated alumina surface has been shown in Figure 4.8.The friction co-efficient for the as received alumina surface has also been included for reference. A low value of friction co-efficient for the laser treated surface can be associated with the surface hardness improvement. In this case, surface hardness increased

significantly (1650 (+50/-50) HV) as compared to as received alumina surface (1100 (+50/-50)). The increase in surface hardness is due to the presence of a dense top layer which is formed because of the high cooling rates of nitrogen gas used during laser texturing.

## 4.2 Replication of a Textured Surface Using PDMS

Forming fine texture features at a surface to impart superhydrophobic characteristics is a slow and costly process and the candidate surfaces for such processes are usually opaque. A simple and inexpensive approach to obtain optically transparent superhydrophobic surfaces is to copy and replicate the features of a textured surface using a transparent polymer like PDMS. Laser textured alumina surface and photo lithographically etched silicon micro post arrays are replicated via PDMS and the resultant surfaces are characterized using different tools.

### 4.2.1 Replication of Laser Textured Alumina Using PDMS

PDMS was used to copy and replicate laser textured alumina surfaces. The protocol followed has been mentioned in section 3.3.

Figure 4.9 shows SEM micrographs of replicated PDMS surface. Since liquid PDMS has excellent rheological properties, it replicated almost exactly the surface texture of laser treated surface. PDMS also exhibits low elastic modulus after solidification [61]. In this case, it behaved like an elastic body during the removal from the laser textured surface. In addition, no rapturing of PDMS replicated surface was observed as evident by the SEM images in Figure 4.9. Figure 4.9(a) shows the overlapped laser irradiated spots in the replicated surface which are very similar to the ones observed in the original surface

(Figure 4.2(a)). Some alumina residue was observed on the replicated PDMS surface which was due to the odd orientation and strong adhesion of whiskers on the laser textured surface with PDMS which caused them to be detached and subsequently be transferred to the replicated surface (Figure 4.9(b)). Figure 4.9 (c, d) indicates the presence of sub-micron texture features, very similar to the ones observed in our laser treated alumina sample (Figure 4.2 (c, d)). Some of the texture detail, however, was lost during the replication process. This was due to the odd orientation and complex geometric shape of some of the features in the laser treated surface.

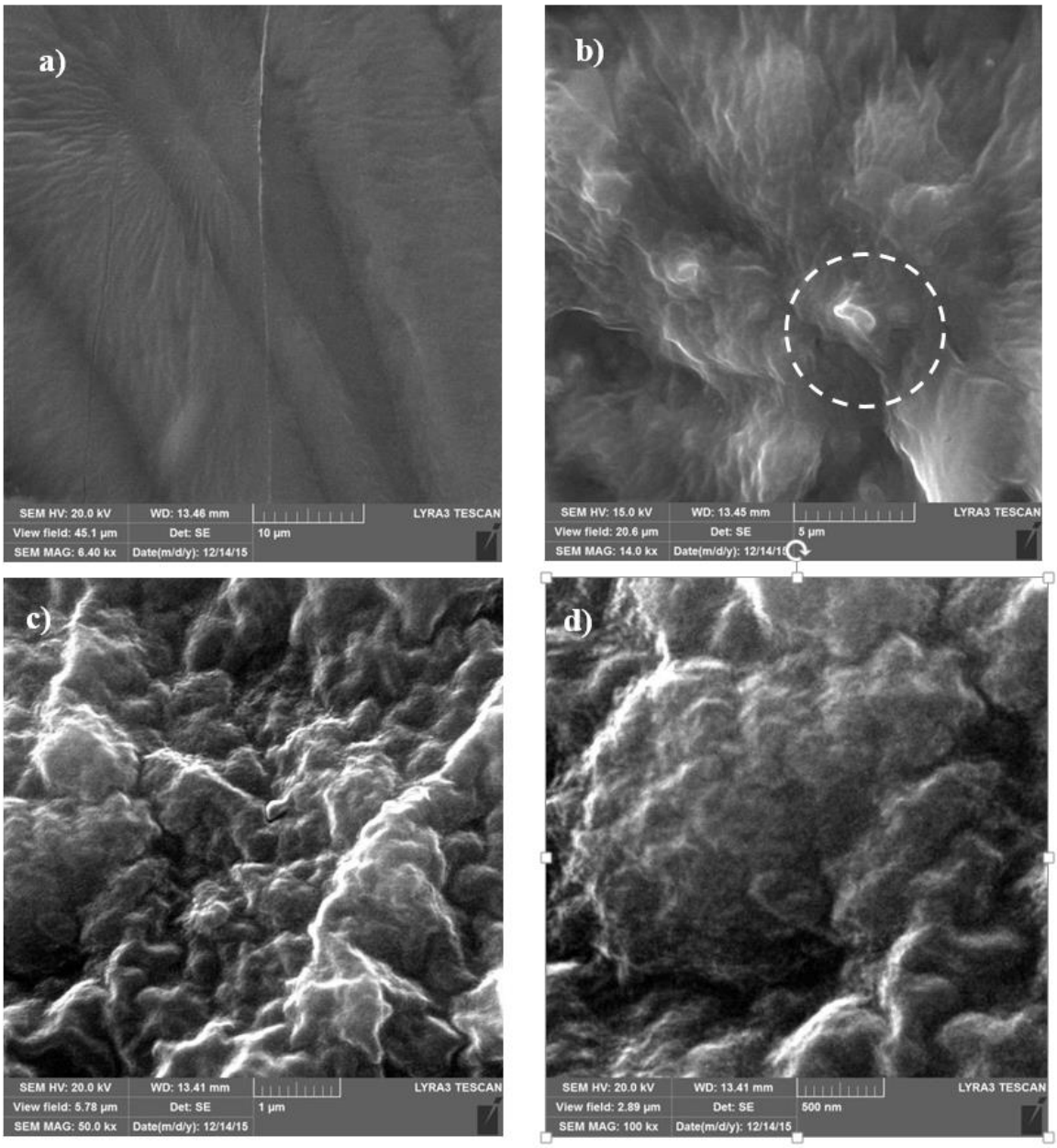


Figure 4.9 SEM micrographs of PDMS surface obtained by replication of laser textured alumina: a) replication of overlapped laser irradiated spots, b) fine size replicated texture with alumina residue (marked circle), d) replication of fine size textures, and d) sub-micron replicated texture

Figure 4.10 show the 3-D optical image of laser textured replicated PDMS surface. It is evident that the replicated surface texture shows identical surface pattern to that of laser textured surface (Figure 4.1).

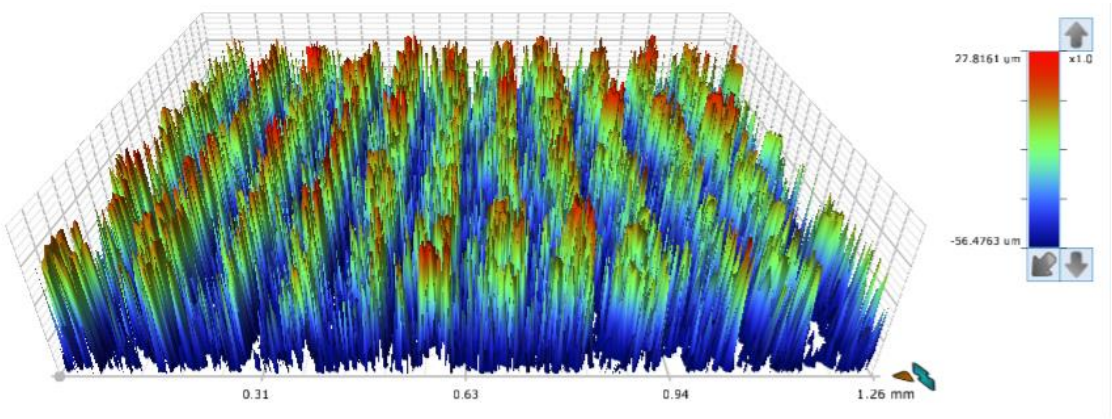


Figure 4.10 3-D optical image of PDMS surface obtained by replication of laser textured alumina

Figure 4.11 shows atomic force microscopy image of the PDMS replicated surface. The general features of the PDMS replicated surface (Figure 4.11(a)) are similar to the laser textured surface (Figure 4.3 (a)). The averaged textures heights of PDMS replicated (Figure 4.11(b)) and laser textured surfaces (Figure 4.3(b)) are almost the same. Consequently, replicated surface has the texture morphology similar to that of the laser textured surface, provided that some fine texture details of the laser treated surface are not observed at the PDMS replicated surface.

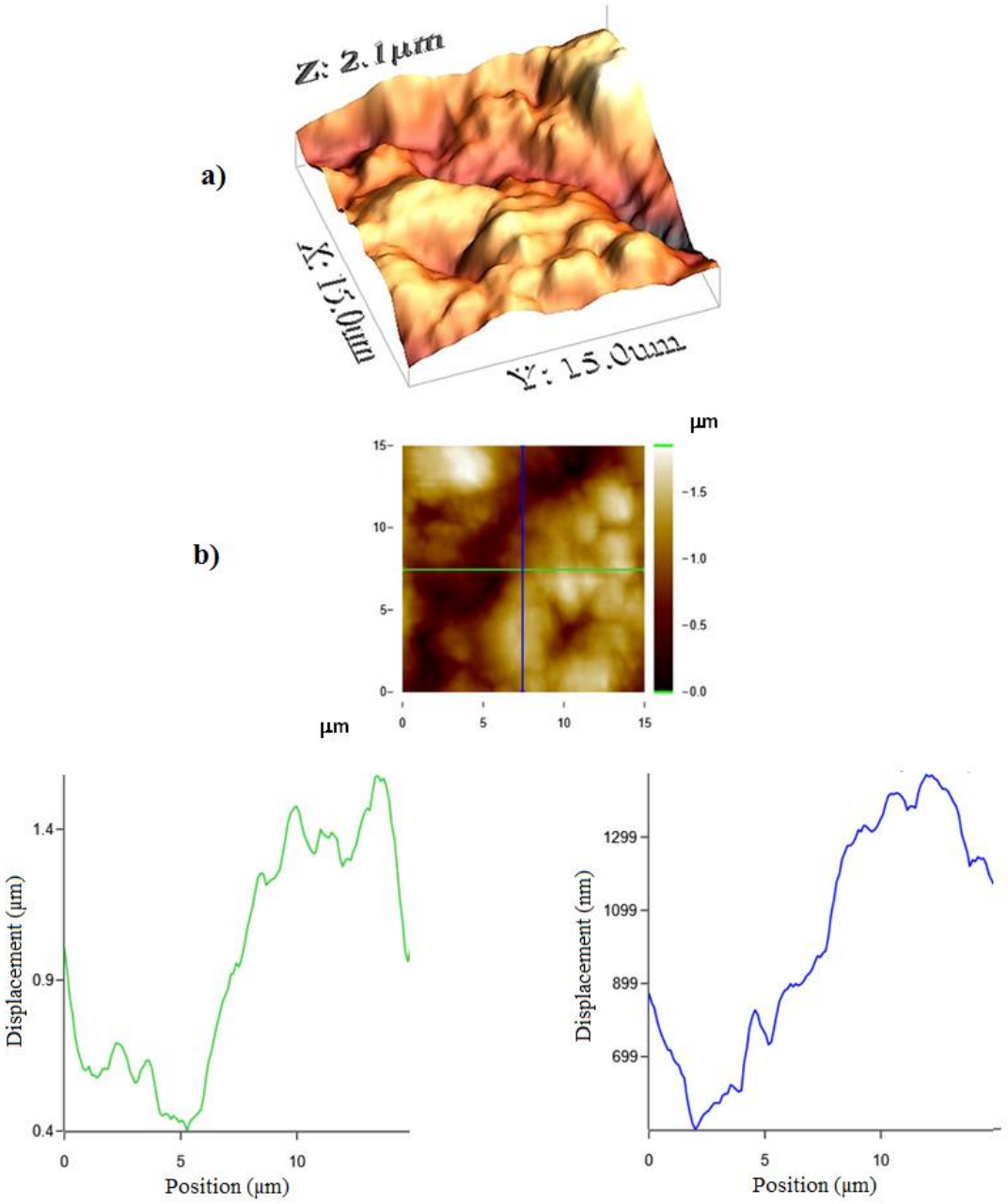


Figure 4.11 Atomic force microscope image of PDMS surface obtained by replication of laser textured alumina: a) 3-D image of replicated PDMS surface, and b) line scan at the replicated surface

Figure 4.12 shows water droplet images obtained for PDMS copied surface (Figure 4.12(a)), and PDMS replicated surface (Figure 4.12(b)). Since the laser irradiated alumina surface had a nearly symmetric texture comprising of peaks and valleys, therefore the value of contact angle observed for both the copied and replicated surfaces is nearly identical. The skewness for laser treated surface, a statistical measure of symmetry, was -0.2 (with 0 being a perfectly symmetric surface).

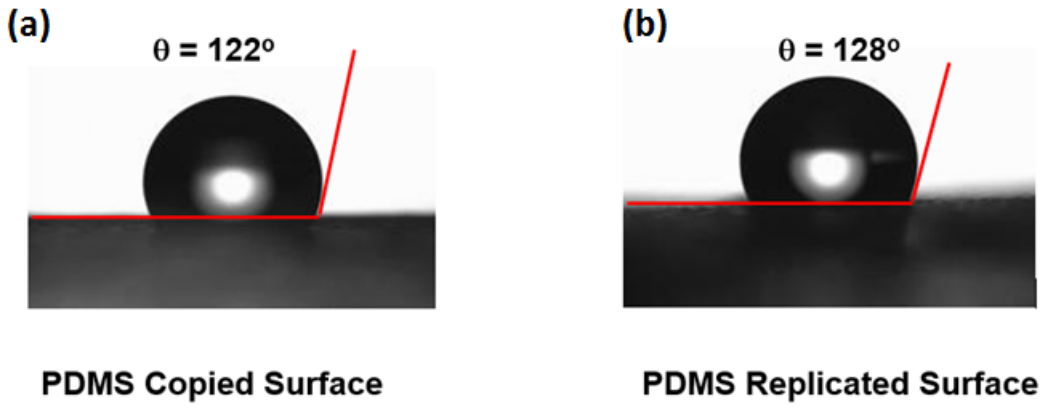


Figure 4.12 Contact angle of water droplet on PDMS surface obtained by(a) copying laser textured alumina and (b) replicating laser textured alumina

The contact angle for the laser treated alumina surface (150°), however, is greater than that of the replicated PDMS surface (128°). This is because of the two reasons; firstly because of the formation of low energy AlN compounds at the laser irradiated surface and secondly, due to the absence of some nano sized whiskers that were present in the laser treated surface but absent in the PDMS replicated surface. Such fine features were not copied during the PDMS replication process. This situation can also be seen from Table 4.2, in which droplet contact angle and hysteresis (CAH=Advancing C.A - Receding C.A) for the surfaces is

given. The hysteresis corresponding to both the copied and replicated PDMS surfaces are slightly higher. In order for the lotus or self-cleaning effect to take place, the contact angle hysteresis should be lower. It will be shown afterwards that the contact angle hysteresis for both the PDMS copied and replicated surfaces can be lowered effectively by depositing a fine layer of functionalized silica nano particles.

Table 4.2 Contact angles measurement results for as received and laser treated alumina surface, and PDMS copied and replicated surfaces

| **Surface** | **C.A (Degrees)** | **CAH (Degrees)** |
|---|---|---|
| Untreated Surface | 65.3 (+1/-1) | 42(+1/-1) |
| Laser Treated Surface | 150.2 (+7/-7) | 18 (+5/-5) |
| PDMS Copied | 122.4 (+0.2/-0.2) | 32(+2.1/-2.1) |
| PDMS Replicated | 128.2 (+1.1/-1.1) | 24(+1.9/-1.9) |

Figure 4.13 shows the optical transmittance of PDMS copied and replicated wafers. The average transmittance for PDMS replicated surface is slightly lower than the PDMS copied surface. This is due to the fact that some of the sub-micron sized features that were embedded in the copied PDMS surface, emerged out for the PDMS replicated surface and contributed to the scattering of light. The emergence of features like this also contributed to the higher contact angle and lower contact angle hysteresis for the PDMS replicated surface.

The transmittance data for as received flat PDMS is also included for the comparison reason. The average transmittance is low for both the PDMS copied and PDMS replicated wafers. It will be shown in next sections that surfaces with ordered texture like those of Micro-Post arrays made by photo-lithography, when replicated by PDMS yield a relatively high transmittance.

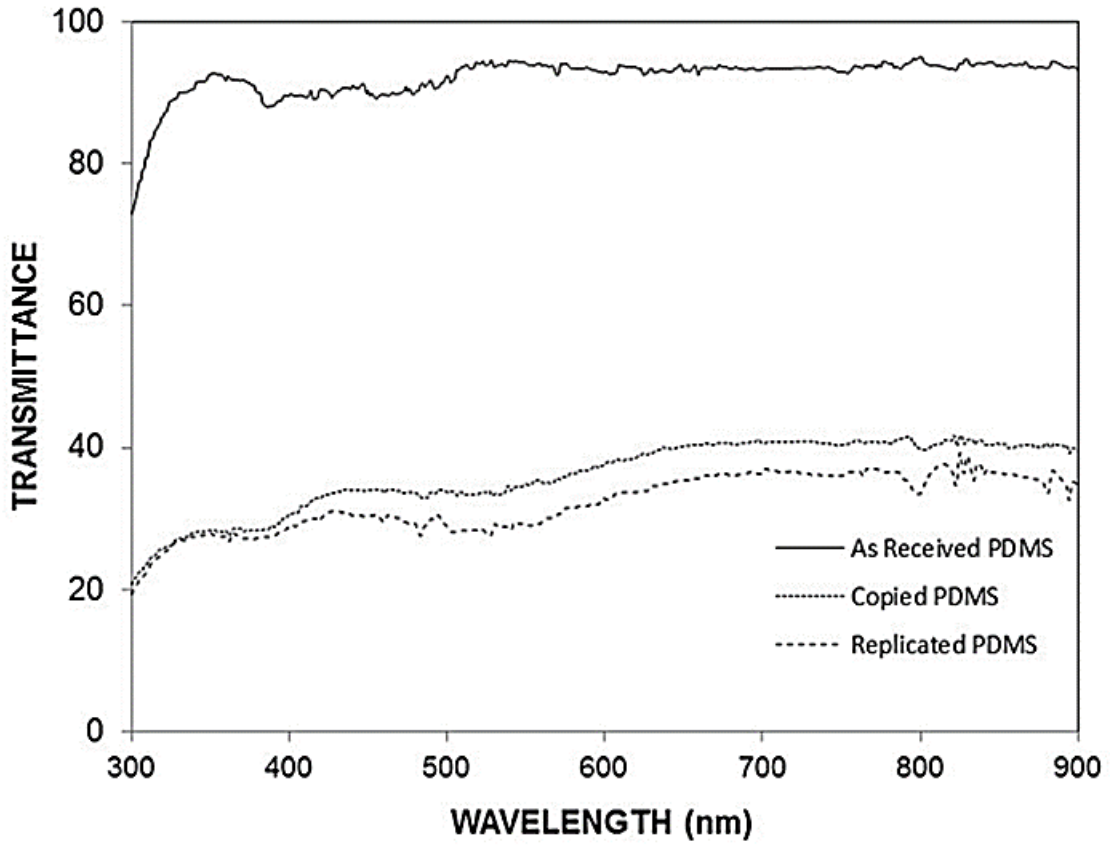


Figure 4.13 UV/Vis transmittance spectra of plane PDMS surface, and PDMS copied and replicated laser treated alumina surface

### 4.2.2 Replicated PDMS Surface with Functionalized Silica Nanoparticle Coating

Since some of the nano-sized whiskers could not be copied from the laser treated alumina sample, synthesized silica nanoparticles were introduced at PDMS copied and replicated surfaces to generate the lotus or self-cleaning effect. It should be noted that nano-size texture is crucial to create a lotus effect on a surface. Figure 4.14 shows SEM micrographs of PDMS replicated surface deposited with functionalized silica nanoparticles.

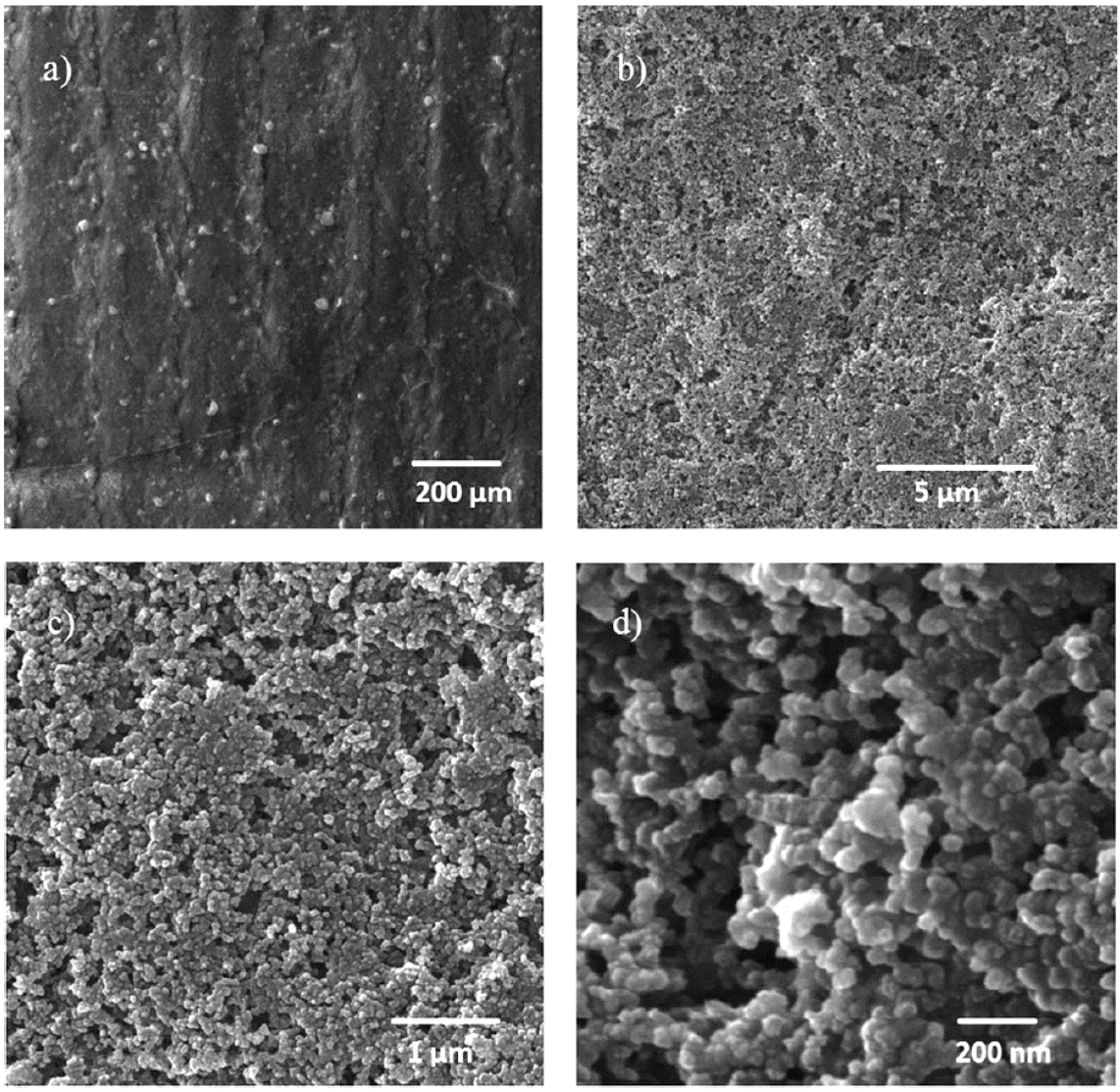


Figure 4.14 SEM micrographs of replicated PDMS surface with functionalized silica nanoparticles: (a, b) extensive coverage of functionalized silica nanoparticles at PDMS replicated surface, (c, d) aggregated functionalized silica nanoparticles

It can be seen from Figure 4.14(b) that the deposited silica particles cover extensively PDMS replicated surface. The average size of the synthesized silica nano particles is in the order of 66nm. Since tetraethyl orthosilicate (TEOS) is used in the synthesis of silica nanoparticles, the functionalized shell distorts the surface roughness of the particles; in

which case, a small increase in the cell size occurs [62]. This can be related to the condensing monomer units, which are growing at a faster rate than the nucleation rate [25]. Since diluted TEOS concentration with ethanol is incorporated during synthesizing silica nanoparticles, the rate of formation of new nuclei is suppressed. This, in turn, resulted in aggregation and adhesion of the particles (Figure 4.14(c, d)). It should be noted that the hydroxyl groups on the functionalized silica nanoparticle surfaces can have different reactivity towards the modifier molecules. Hence, modifier silane results in side reactions and condensation on the silica surface [63].

Figure 4.15 shows AFM images of PDMS replicated surface after deposition of functionalized silica nanoparticles. The presence of silica nanoparticles is evident from the line scan (Figure 4.15(b)). In this case, small peaks arising due to silica nanoparticles are superimposed onto the larger peaks arising to create a two tiered or hierarchal texture. It has been studied that the presence of this dual scale roughness is necessary to create a superhydrophobic surface with lotus effect [64]. SEM micrographs (Figure 4.14) and AFM images (Figure 4.15) also show the absence of loose silica particles. It can, therefore, be concluded that functionalizing silica particles prior to deposition onto PDMS replicated surface improved the adhesion between the particles and the surface.

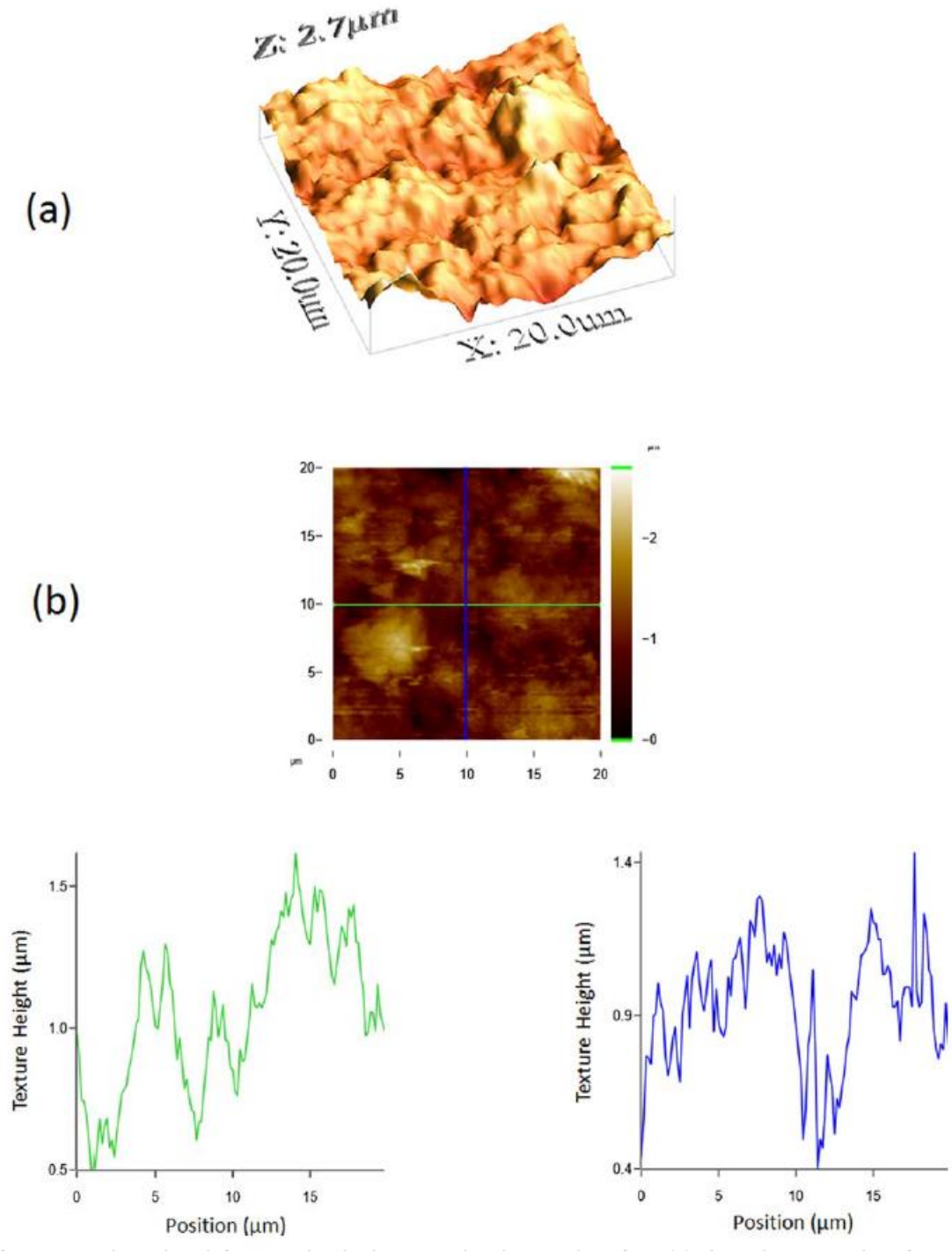


Figure 4.15 AFM image of replicated PDMS surface with functionalized silica nanoparticles:(a) three-dimensional surface texture, and (b) line scan at the surface

Figure 4.16 shows FTIR data for PDMS replicated surface deposited with functionalized silica nanoparticles. The FTIR data for plain PDMS sample has also been included for reference. In general, two groups of data can be observed, namely, Si-Methyl (Si-Me) and Siloxane (Si-O-Si) groups. A doublet at 1066 $cm^{-1}$ and 1015 $cm^{-1}$ correspond to asymmetric stretching vibrations of siloxane groups [65]. The peak at 1250 $cm^{-1}$ signifies Si-C deformations in Si-Methyl groups [66]. The presence of absorption peak at 2960 $cm^{-1}$ and 2902 $cm^{-1}$ corresponds to $–CH_3$ and $-CH_2$ (asymmetric) bend stretching vibration [67]. The peak at 800 cm-1 is related to Si-C stretch in Si-Methyl groups. No -OH peak is observed for the replicated PDMS samples with functionalized silica nanoparticles which indicates that the silica nanoparticles are fully covered with grafted groups. The relative intensities of the peaks corresponding to $-CH_3$ and $-CH_2$ vibrations at 2960 $cm^{-1}$ and 2902 $cm^{-1}$ are higher for functionalized silica particle deposited surfaces. The increase in intensity indicates that the surface of the silica nanoparticles is covered with the methyl terminated groups.

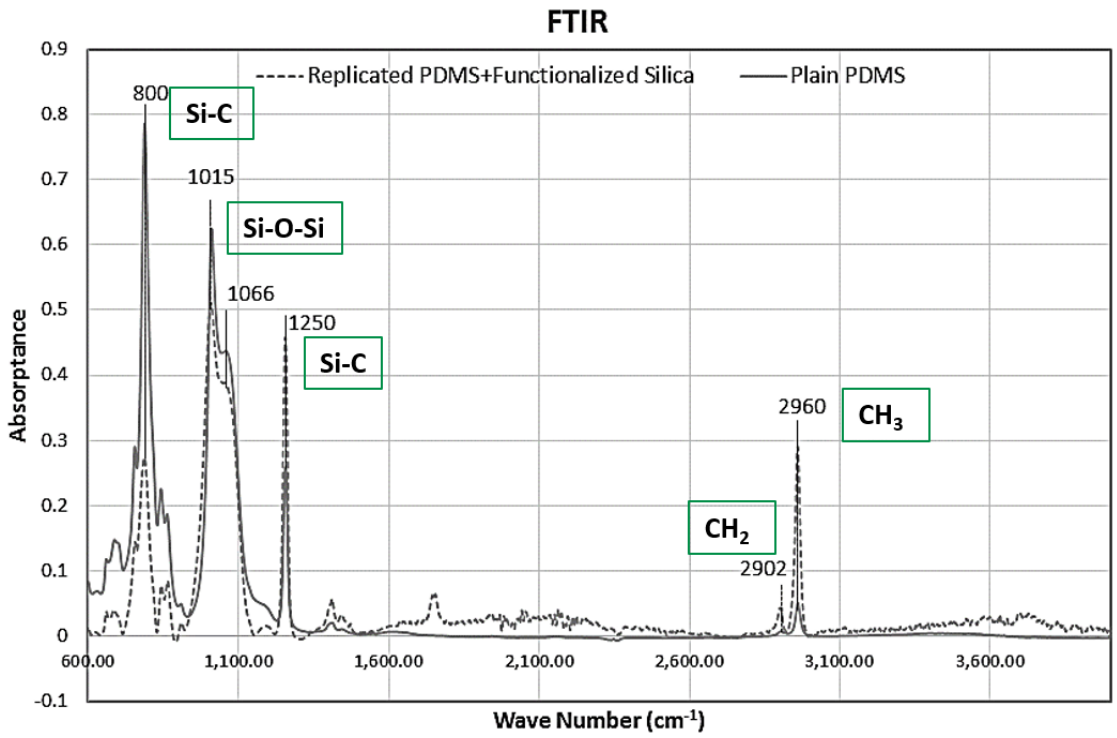


Figure 4.16 FTIR spectra of plain PDMS and replicated PDMS sample with functionalized silica nanoparticles

Figure 4.17 shows the UV-Vis transmittance data for PDMS copied, replicated and functionalized silica particles deposited surfaces. The transmittance for PDMS surfaces deposited with functionalized silica nanoparticles is slightly lower than replicated surfaces in the wavelength range of 300 nm to 550 nm. For longer wavelengths, the transmittance increases for functionalized silica particle deposited PDMS surfaces.

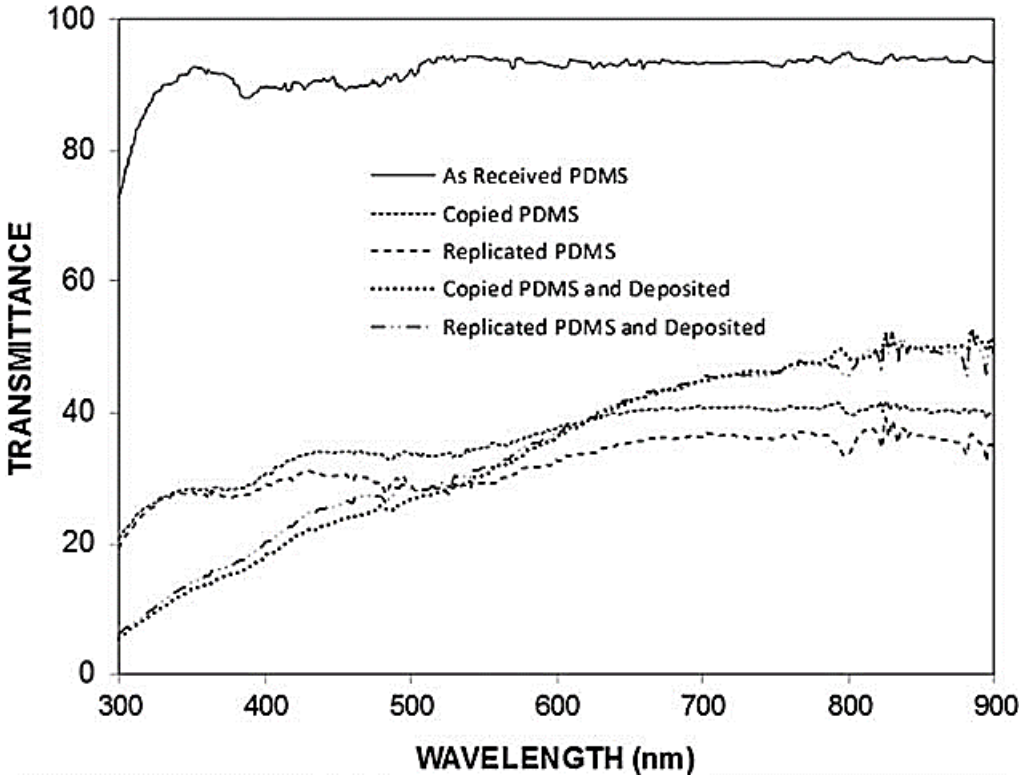


Figure 4.17 UV/Vis transmittance spectra of as received PDMS wafer, PDMS copied and replicated surfaces, and copied and replicated PDMS surfaces with functionalized silica nanoparticles

Table 4.3 summarizes the contact angle data for functionalized silica nanoparticles deposited PDMS surfaces.

Table 4.3 Contact angle data for PDMS copied and replicated surfaces deposited with functionalized silica nanoparticles

| **Surface** | **C.A (Degrees)** | **CAH (Degrees)** |
|---|---|---|
| PDMS Copied Surface + Functionalized Silica Nanoparticles | 157 (+1.5/-1.5) | 4.0(+3.3/-3.3) |
| PDMS Replicated Surface + Functionalized Silica Nanoparticles | 155.5 (+0.8/-0.8) | 2.6 (+1.9/-1.9) |

Deposition of functionalized silica nanoparticles on PDMS copied and replicated surfaces significantly increased the CA and reduced the CAH. This is due to the creation of a hierarchal structure as seen in the AFM scans in Figure 4.15. Since the PDMS copied and replicated surfaces had a similar contact angle, the contact angle after deposition of silica nanoparticles remains close as well. Figure 4.18 shows the water contact angles for the PDMS surfaces deposited with functionalized silica nanoparticles.

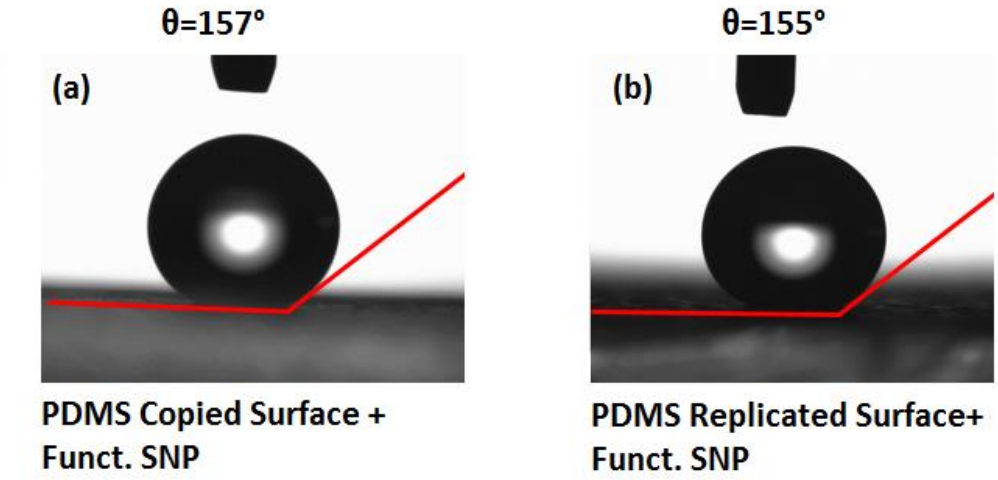


Figure 4.18 Contact Angle of water droplet on (a) PDMS copied surface with functionalized silica nanoparticles(b) PDMS replicated surface with functionalized silica nanoparticles

### 4.2.3 Replicated PDMS Micro-Post Arrays

Micro Post Arrays with square tops having length a=10 µm, height h=10 µm, and a varying edge to edge spacing b=10, 25 and 50 µm were etched on a silicon wafer using standard photo-lithography procedure. PDMS (polydimethylsiloxane) was used to copy and replicate the micro-post array texture. The textured silicon wafers were first silanized with Octadecyltrichlorosilane. PDMS was used to copy the textured silicon wafer. The copied PDMS sample was silanized with PFOTS via vapor deposition prior to second casting with PDMS. Figure 4.19 shows the SEM micrographs for the samples obtained after double casting with PDMS.

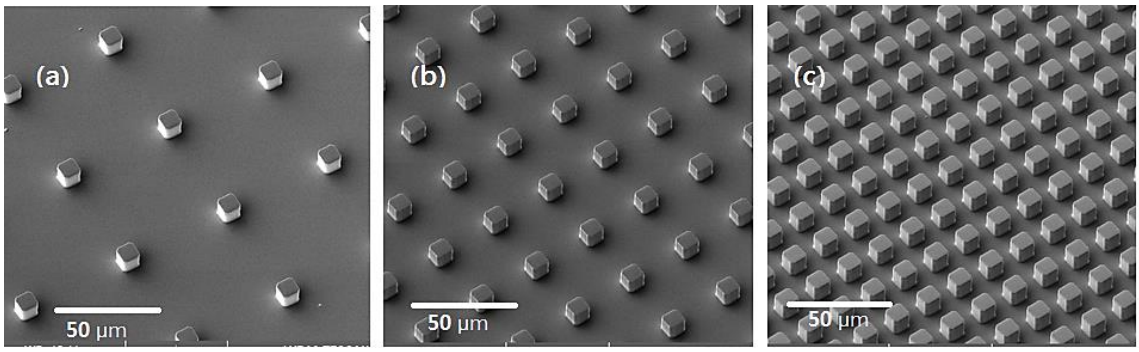


Figure 4.19 SEM micrographs of replicated PDMS Micro post arrays with post spacing of (a) 50 µm, (b) 25 µm, (c) 10 µm

It can be seen from Figure 4.19 that the procedure adopted allowed for the successful replication of silicon micro post array samples. The texture was free from any defects and had good dimensional stability. Table 4.4 gives the roughness ratio *r* ($r = 1 + \frac{4ah}{(b+a)^2}$) and fraction of area of the surface occupied by square post tops $\phi$ ($\phi = \frac{a^2}{(a+b)^2}$).

Table 4.4 Roughness ratio *r* and fractional posts top area $\phi$ for the PDMS micro-post arrays with pitch of 10 µm, 25 µm, and 50 µm

| **Pitch (µm)** | **r** | **ϕ** |
|---|---|---|
| 10 | 2 | 0.25 |
| 25 | 1.326 | 0.0816 |
| 50 | 1.111 | 0.0277 |

Static and dynamic water contact angle measurements were performed for the three samples and the results are summarized in the Table 4.5.

Table 4.5 Contact angle results for replicated PDMS micro post arrays

| **Sample** | **C.A.(deg)** | **Tilt Angle** | **CAH ($\theta_{adv} - \theta_{rec}$)** |
|---|---|---|---|
| 10um pitch | 149.9 | 20 | 160.8-118.4=42.4 |
| 25um pitch | 152.1 | 11 | 162.1-137=25.1 |
| 50um pitch | 163.8 | 4 | 165-153.6=11.4 |

Figure 4.20 shows the water droplets placed on the micro post array PDMS surfaces.

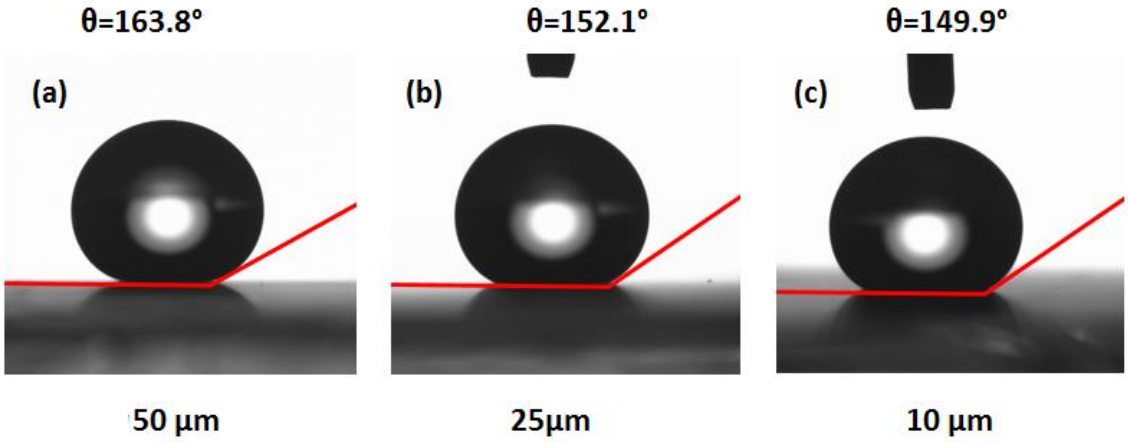


Figure 4.20 Water droplet on replicated PDMS micro post arrays with post spacing of (a) 50 µm, (b) 25 µm, (c) 10 µm

The contact angle is highest for the surface with 50 µm post spacing and then follow the surfaces with post spacing of 25 µm and 10 µm. The increase in contact angle with increasing pitch or post spacing is due to the decreasing percent area of solid in contact with water. This is represented by the value $\phi$ in Table 4.4. Large air pockets, forming beneath the droplet, are responsible for the increase in the value of contact angle and a decrease in the value of contact angle hysteresis and tilt angle. Although the contact angle

and its hysteresis depend on the surface roughness ratio as well, but here the dominating factor is $\phi$ which represents the percent surface area in contact with water. It can be seen from Table 4.4 that the value of $\phi$ decreases by a factor of 10 while the surface roughness ratio decreases by a factor of 2 as we move from 10 μm pitch to 50 μm pitch. The increase in surface roughness ratio has other consequences as well. The number of pinning sites are substantially increased as the surface roughness ratio increases which cause the droplets to stick to the surface. This is also one of the reason for the large contact angle hysteresis and tilt angle for the surface with 10 μm pitch. One advantage for the surface with 10 μm pitch is that the droplet always remains in the cassie-bexter state whereas for the surface with 50 μm pitch, the droplet easily goes into the wenzel state if the size of the droplet is small enough. This is an undesirable consequence for surfaces with large pitch or post spacing.

In terms of superhydrophobic characteristics, the PDMS micro post array surfaces are much superior to the ones obtained by replication of laser textured workpieces. This is due to the fact that the water droplet remains in the Cassie-Bexter state (with air pockets beneath the droplet) for these surfaces whereas for the laser textured replicated ones, the droplet goes into the wenzel state (fully wetting state with no air pockets beneath the droplet). The reason for the droplet to fully wet the PDMS replicated surfaces (laser textured ones) is due to the small texture heights (only 2um) which cause the droplet to penetrate the peaks and be in contact with the base PDMS surface. The peak to valley distance for our micro post arrays is in the order of 10um thus enabling the droplets to be in the Cassie-Bexter state. Figure 4.21 gives the UV/Vis transmittance for these surfaces.

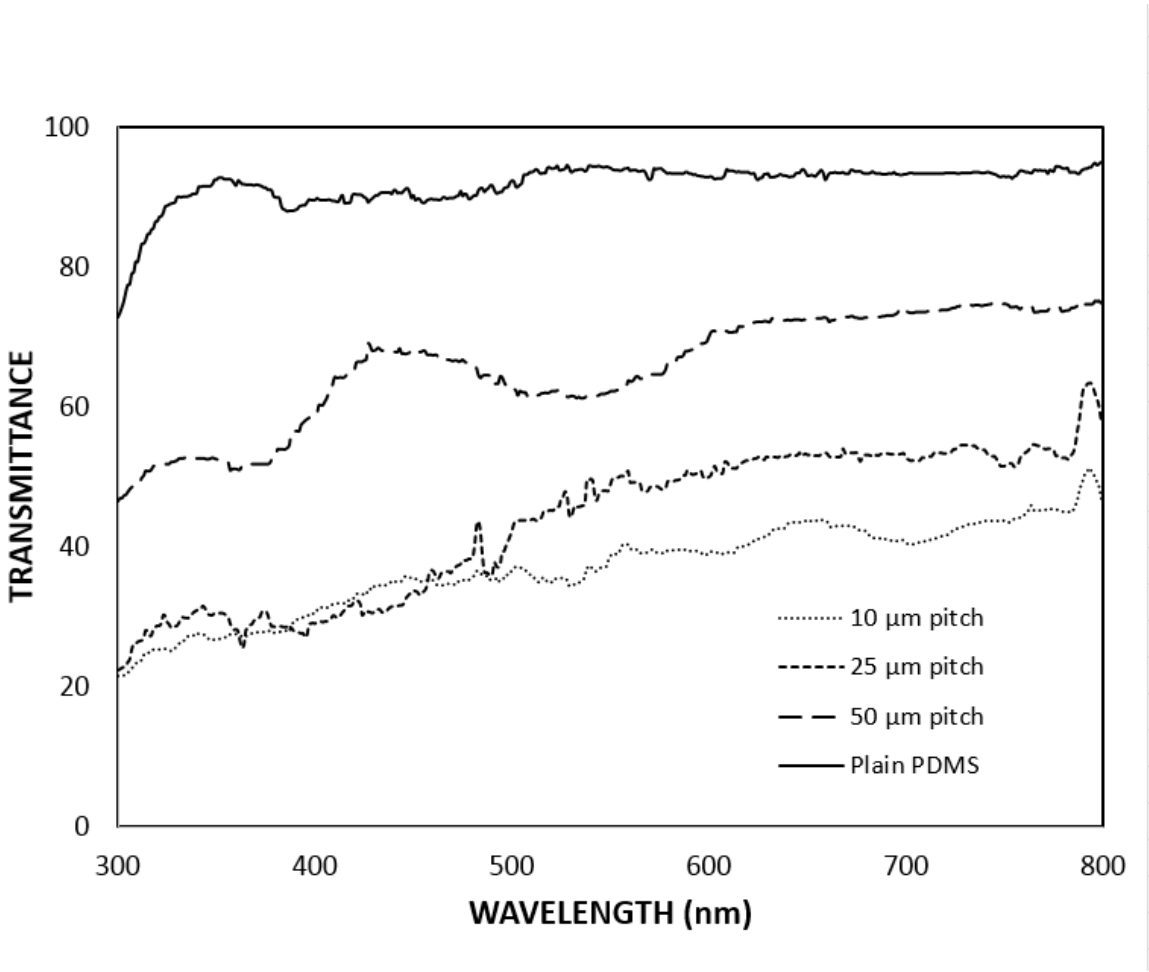


Figure 4.21 UV/Vis transmittance spectra for plain PDMS and replicated PDMS micro post arrays with 10um, 25um, and 50um post spacing

The transmittance observed is highest for the surface with post spacing of 50um and then follows the surface with 25um and 10um post spacing. This is associated with increasing roughness ratios of these surfaces which cause scattering of the incident light.

## 4.3 Silica Nanoparticle Coating on Glass Slide

The second part of this study focuses on the development of superhydrophobic and self-cleaning glass surfaces. Silica nanoparticles are used to generate a texture at the glass surface. Synthesized and functionalized silica nanoparticles are deposited via solvent deposition and the superhydrophobicity and optical transmittance of the resultant surfaces is analyzed. As received silica colloids are convectively assembled at the glass surface to obtain a fine layer of silica nanoparticles. After functionalization with OTS, the obtained surfaces are checked for non-wetting characteristics and optical transmittance.

### 4.3.1 Solvent Deposition of Silica Nanoparticles

Functionalized silica nanoparticles, synthesized by the procedure mentioned earlier, were deposited onto the clean glass slides. Figure 4.21 show the SEM micrographs for the resultant surfaces.

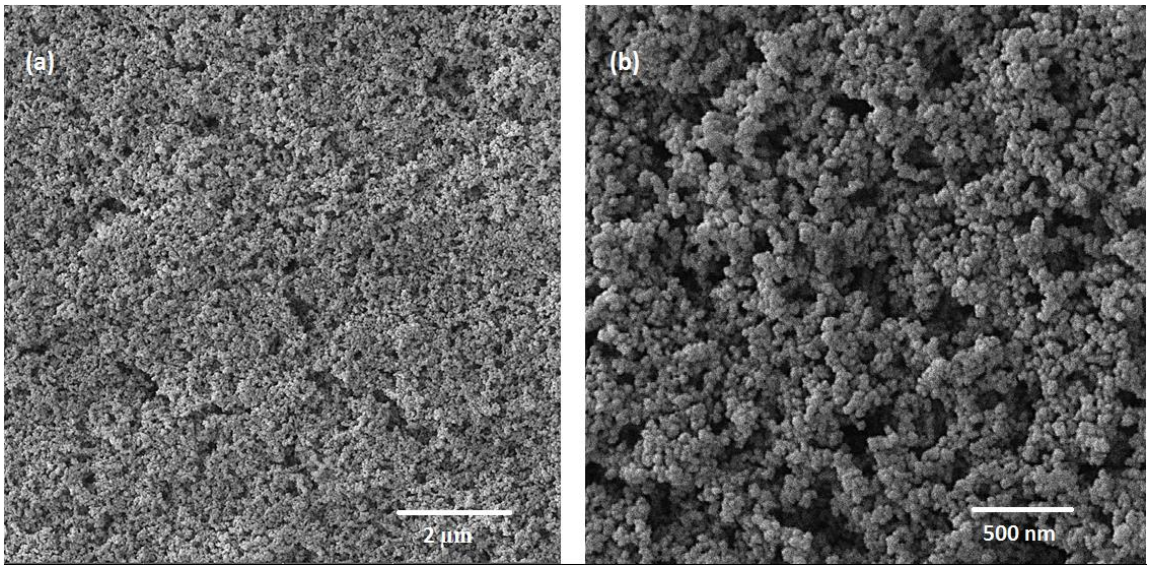


Figure 4.22 SEM micrographs of glass surface deposited with functionalized silica nanoparticles (a) extensive coverage of the silica nanoparticles (b) porous network formed by the deposition of silica nanoparticles

Figure 4.22 (a) shows that the silica nanoparticles extensively cover the surface of the glass slide, leaving no gaps in the coating. A close examination of the coating (Figure 4.22(b)) reveals the presence of a hollow structure with small air pockets in between the silica nanoparticles. In between these pockets, the silica nanoparticles exist in the form of agglomerates. Figure 4.23 shows the contact angle of water droplet on this surface.

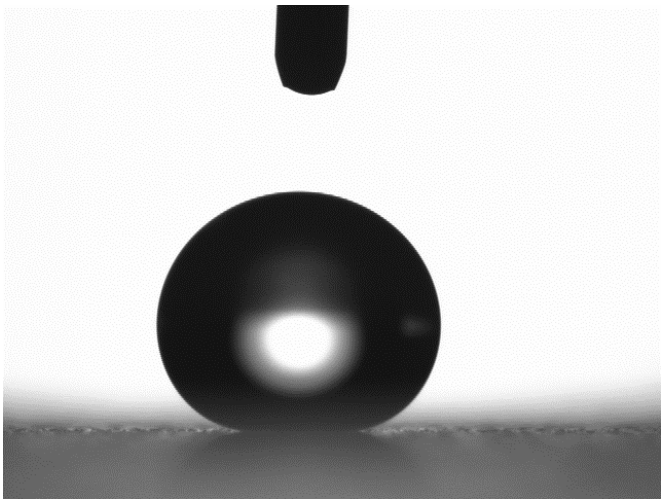

Figure 4.23 Water droplet on glass surface deposited with functionalized silica nanoparticles

The CA for water is 170°± 2° and the CAH is less than 1°. Such high values of CA and low values of its hysteresis is due to the formation of a porous network of silica nanoparticles (Figure 4.22 (b)). The presence of such small air pockets ensure that the droplet never penetrates in between the texture and always rolls-off at very small tilt angles (<1°). Another reason for such a high value of CA can be attributed to the complete absence of hydroxyl groups as evident in the FTIR (Figure 4.16). Figure 4.24 shows the UV/Vis transmittance spectra for the plain glass slide and glass slide deposited with functionalized silica nanoparticles.

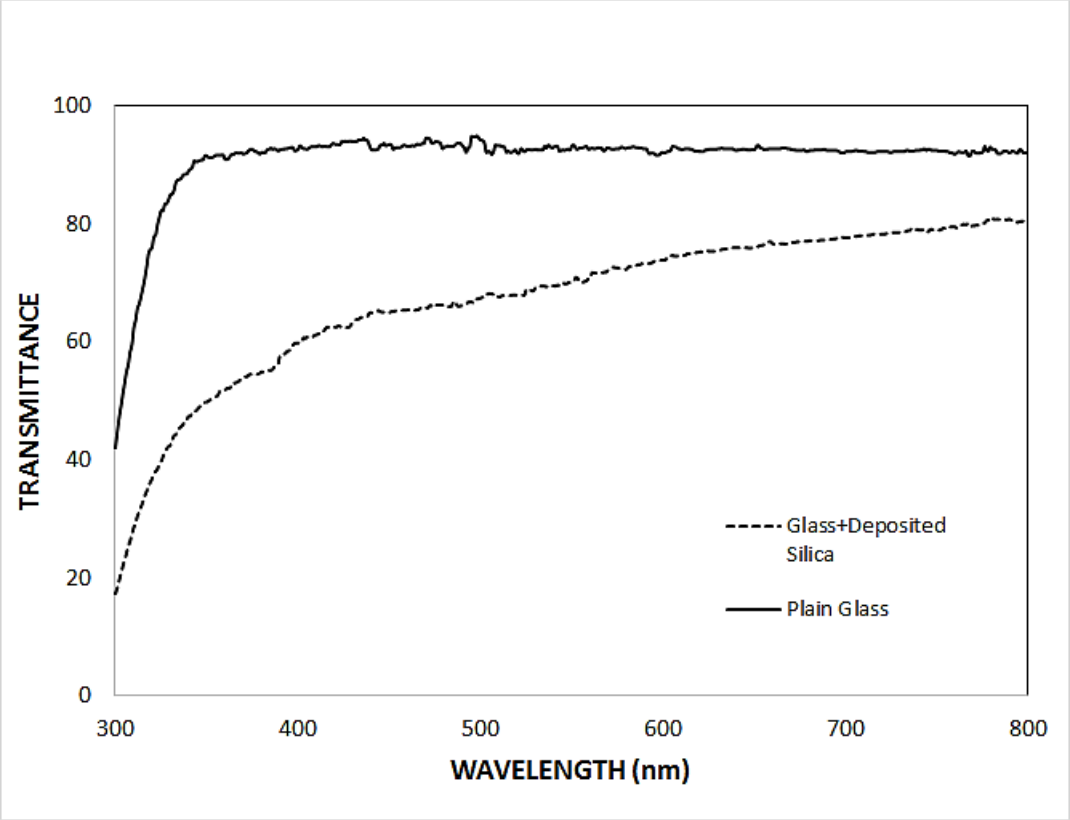


Figure 4.24 UV/Vis transmittance spectra for plain glass surface and glass surface deposited with functionalized silica nanoparticles

In comparison to the plain glass slide, the transmittance for the silica nanoparticle deposited glass slide is low in the wavelength range of 300-500nm. The transmittance for the coated glass slide improves for longer wavelengths.

### 4.3.2 Dip Coating in Silica Particles

A fine layer of silica particles was convectively assembled onto the glass slide by dip coating using the procedure mentioned in the experimental section. After baking, the silica particles were functionalized with OTS. Figure 4.25 shows SEM micrographs of glass

surface with silica particles coating. The silica coating is discontinuous with voids in between as seen in Figure 4.25(a). The formation of voids is due to the large withdrawal speed (exceeding the monolayer formation speed). At higher withdrawal speeds, the particle influx is not enough to form a complete monolayer [68]. Figure 4.25(b, c) shows a close up view of the silica coating on glass surface. The arrows indicate the areas where the coating appears to be multi-layered. The formation of multilayers is due to the pinning of the meniscus around larger diameter silica particles (220nm). The meniscus then does not wet the full width of the substrate and causes the particles to pack into multi layers at pinning sites [69]. The silica coating transitions from multi to mono layer as we move away from the bigger diameter particles as shown by a circle in Figure 4.25(d). The surface coverage ratio of silica particles calculated (at 10.0kx magnification) is in the order of 0.63 ± 0.05. A small deviation indicates that the voids are uniformly distributed throughout the coating.

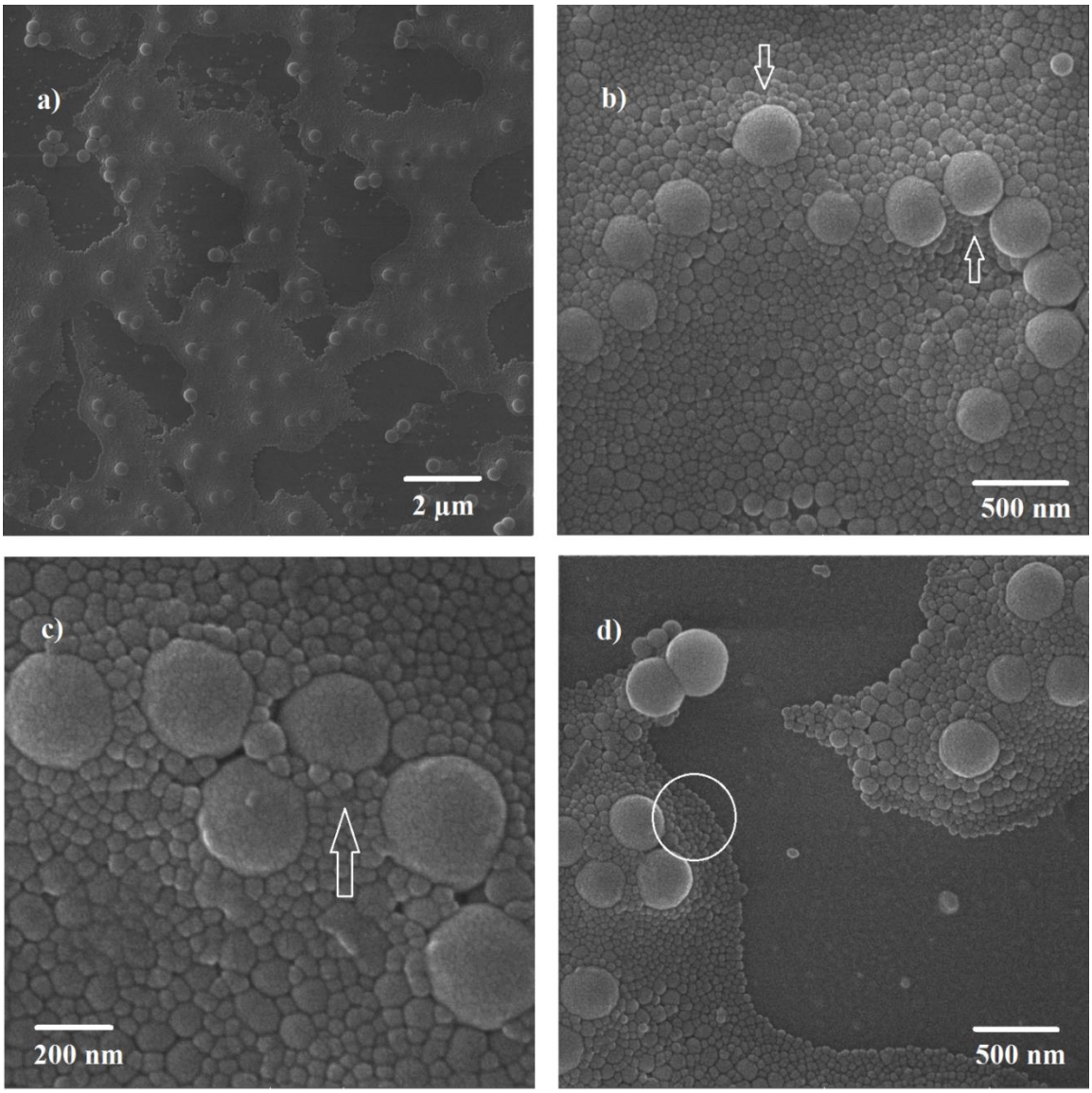


Figure 4.25 SEM micrographs of glass surface coated with silica particles and functionalized with OTS (Octadecyltrichlorosilane) (a) presence of voids in the coating (b) and (c) formation of multilayers around larger diameter particles as indicated by arrows (d) multilayer to monolayer transition as indicated by a circle

Figure 4.26 shows AFM image of the silica particle coated glass surface.

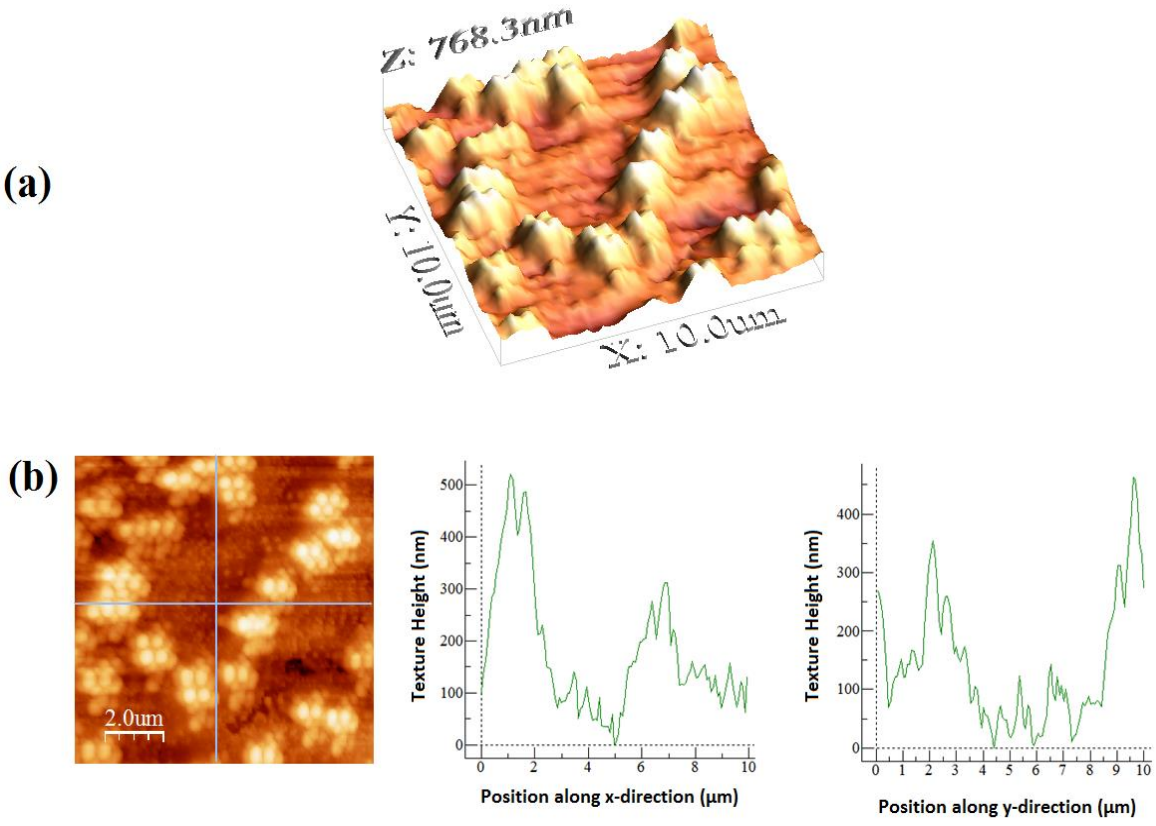


Figure 4.26 AFM images of glass surface coated with silica particles and functionalized with OTS (Octadecyltrichlorosilane): a) 3-dimensional surface texture and b) surface line scan along x and y directions

The 3-d surface texture is shown in Figure 4.26(a) and the line scans along the x and y directions are shown in Figure 4.26(b). The maximum feature height as observed in Figure 4.26(a) is 768.3nm which indicates that the coating is multilayered since the largest particle diameter is 220nm. The average roughness of the coating is in the order of 109.6 nm. The line scans in Figure 4.26(b) show small peaks and valleys created by the inclusion of

smaller diameter nano particles. The result is a hierarchal texture whereby the micro scale roughness is provided by the larger diameter silica particles (220nm) and the nano scale roughness by smaller particles (70nm and 35nm). Fourier transform infrared spectroscopy (FTIR) data for silica particles coated glass surfaces, functionalized with OTS, is shown in Figure 4.27.

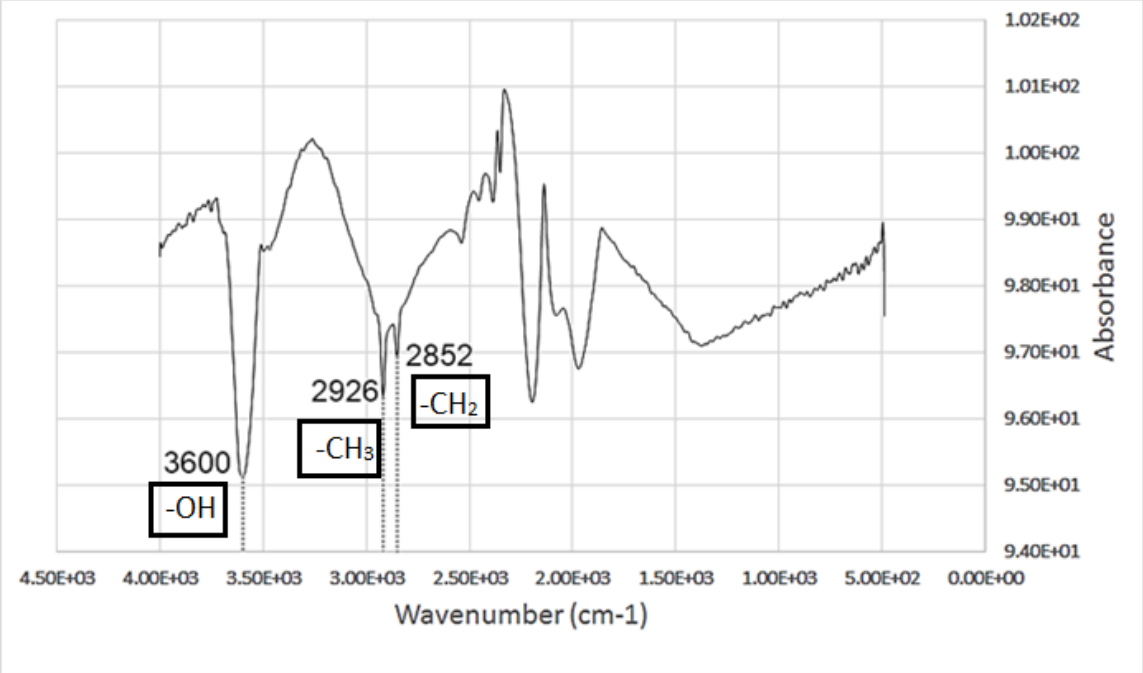


Figure 4.27 FTIR spectrum for glass surface coated with silica particles and functionalized with OTS (Octadecyltrichlorosilane)

The peak at 3600 $cm^{-1}$ represents the stretching vibration of -OH groups [70]. Symmetric and asymmetric stretching of $CH_2$ and $CH_3$ peaks take place at 2852 and 2926 $cm^{-1}$ respectively. These peaks arise due to the functionalization of silica coated glass surfaces with OTS [71]. Figure 4.28 show the contact angle of water droplet on the silica coated surface after functionalization with OTS. The WCA observed is 142° with CAH of 67.7° (160.7°-93°) and a roll off angle of 52°.

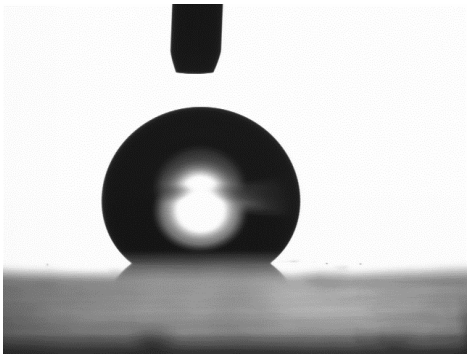

Figure 4.28 Water droplet on glass surface coated with silica particles and functionalized with OTS (Octadecyltrichlorosilane)

The CAH and roll-off angle values are quite high which indicates that the droplet is in the wenzel (complete wetting) state. This may be due to the presence of large voids in the silica particle coating as observed in the SEM micrographs (Figure 4.25(a)). Another possible explanation for the stiction of water droplet to the surface can be the presence of hydroxyl groups as indicated by FTIR (Figure 4.27). The -OH signal is coming either from the silica particles or from the glass substrate. In both cases, it indicates that the surface (glass or silica particles) is not fully functionalized with OTS. Figure 4.29 shows the UV/Vis transmittance spectra for the glass surface coated with silica particles and functionalized with OTS.

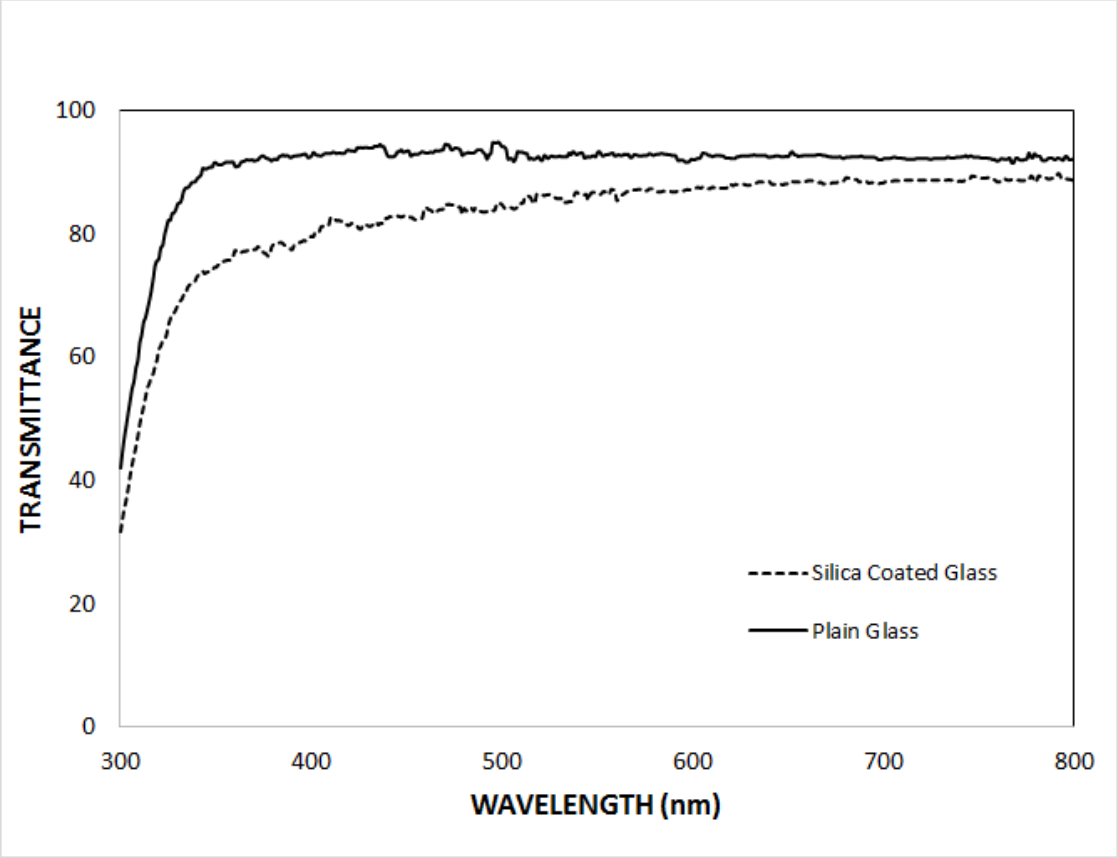


Figure 4.29 UV/Vis transmittance spectra for glass surface coated with silica particles and functionalized with OTS (Octadecyltrichlorosilane)

The transmittance of the silica coated glass surface is fairly high and becomes much closer to that of actual glass at longer wavelengths.

## 4.4 Oil Impregnation of Textured Surfaces

Filling the texture of a superhydrophobic surface by some lubricant can impart some beneficial properties to the surface and can enable it to overcome many of the limitations associated with conventional superhydrophobic surfaces. The glass surfaces obtained after dip coating in silica particle suspension and functionalization with OTS, are impregnated with silicon oil in this study.

### 4.4.1 Oil Impregnation of Silica Particle Coated Glass Surface

Figure 4.30 shows the contact angle of silicone oil on glass surface coated with silica particles and functionalized with silica particles.

Figure 4.30 Silicone oil droplet on silica coated glass surface functionalized with OTS(Octadecyltrichlorosilane)

It can be seen in Figure 4.30 that the oil completely wets the surface with a C.A of nearly 0°. On the other hand, the surface shows a C.A of 142° for water (Figure 4.28). Both of these conditions are necessary in order to have a stable oil film encapsulating the surface texture [22].

In order for the impregnated surface to shed the droplets at small tilt angles with little or no hysteresis, a thin lubricating film must be present underneath as well as outside the droplet. This can be achieved if the spreading co-efficient of oil on surface in the presence of air and water is equal to or greater than zero i.e. $S_{os(a)}= (\gamma_{sa} - \gamma_{so} - \gamma_{oa}) \geq 0$ and $S_{os(w)}= (\gamma_{sw} - \gamma_{so} - \gamma_{ow}) \geq 0$ [26], where $\gamma$ is the interfacial tension and the subscripts s, o, a, and w denote surface, oil, air and water phases respectively. If for a surface, $\theta_{os(a)}=0$ and $\theta_{os(w)}=0$, then by Young's equation of contact angle, both conditions ($S_{os(a)} \geq 0$ and $S_{os(w)} \geq 0$) are satisfied. Indeed, for our surface, both contact angles were found to be zero and a thin film encapsulated the texture, thereby allowing the water droplets to slide at near to zero tilt angles with negligible hysteresis. Figure 4.31 shows such an image of water droplet making contact at an angle of 104° with our lubricant impregnated surface. At the periphery of the droplet, the lubricant is pulled up (as seen in Figure 4.31) in order to satisfy the surface tension force balance.

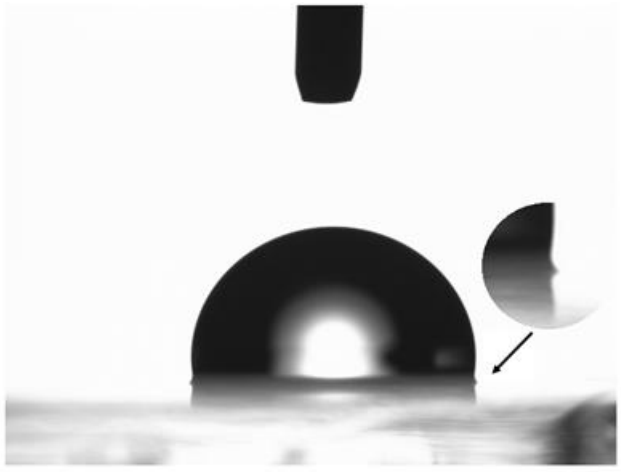

Figure 4.31 Water droplet on silicone oil impregnated surface

It is possible for the lubricant to cloak the water droplet if the spreading coefficient for the oil-water-air system is greater than zero. For our case, $S_{ow(a)}$= 5.57 $mNm^{-1}$ (calculated in Table 4.6) so the water droplets will be encapsulated by a thin silicone oil film. This is an undesirable effect which may lead to the loss of lubricant as the droplets are being shed away.

Table 4.6 Spreading Coefficient for silicone oil-water-air system

| **Spreading Coefficient** | **Expression** | **Interfacial Tensions(mN/m)** | | | **Calculated Value** |
|---|---|---|---|---|---|
| $S_{ow(a)}$ | $\gamma_{wa} - \gamma_{ow} - \gamma_{oa}$ | $\gamma_{wa}$ | $\gamma_{ow}$ | $\gamma_{oa}$ | 5.57 $mNm^{-1}$ |
| | | 72.2 | 46.18 | 20.45 | |

Figure 4.32 shows UV/Vis transmittance spectra of plain glass and glass surface impregnated with silicone oil.

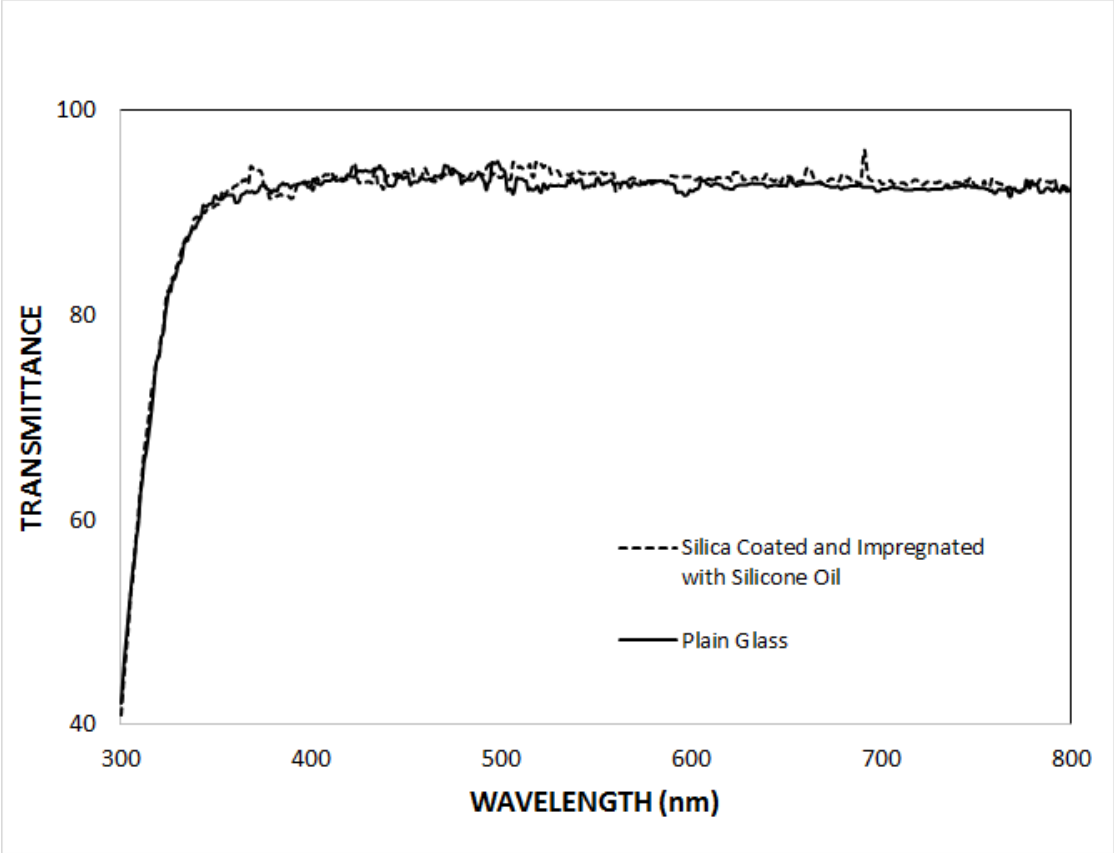


Figure 4.32 UV/Vis transmittance spectra for plain glass and silicone oil impregnated glass surface

The lubricant provides a very smooth interface and reduces the scattering of the incident light due to which the transmittance of impregnated surface is relatively high.

## 4.5 Characterization of Dust

The last part of the thesis focuses on the characterization of dust particles collected from Dhahran, KSA area. The dust particles have been characterized using SEM, EDS, XRD, and Micro-CT. The interaction of dust particles with oil on silicone oil impregnated surfaces has also been discussed. Figure 4.33 show the SEM micrographs of the collected dust particles.

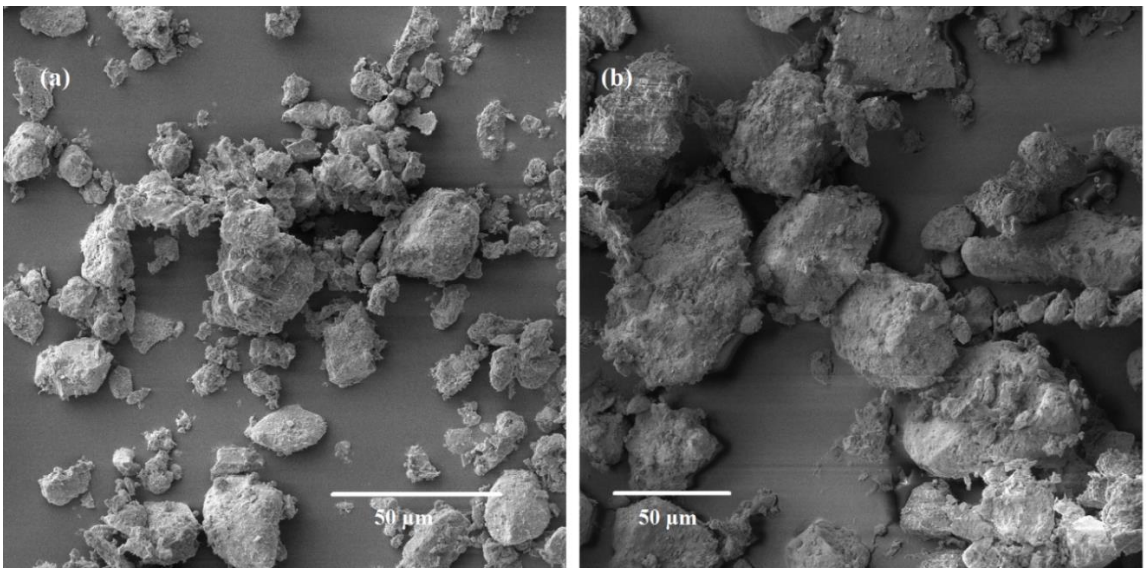


Figure 4.33 SEM micrographs of the dust particles

The dust particles vary greatly in length, ranging from 1 µm to over 100 µm. The shape of the particles also shows a lot of variation. Ellipse fitting on the particles shows that the mean particle aspect ratio is 1.37±00.26 while the shape factor is 1.41±0.16.

In order to determine the elemental composition of the particles, EDS analysis was carried out and the results are presented in Figure 4.34.

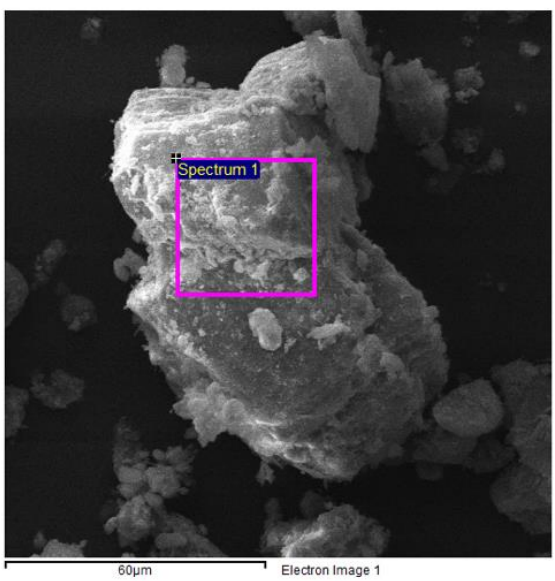


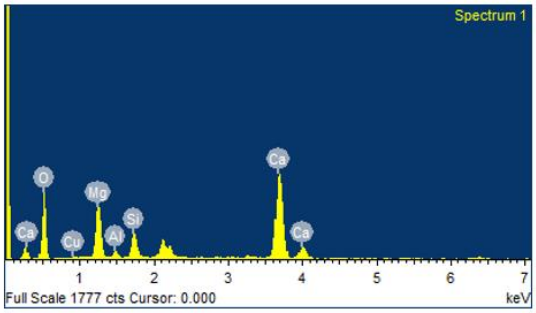


| Element | Wt% | At% |
|---|---|---|
| O K | 60 | 75.52 |
| Mg K | 11.4 | 9.45 |
| Al K | 1.28 | 0.96 |
| Si K | 4.16 | 2.98 |
| Ca K | 20.24 | 10.17 |
| Cu K | 2.92 | 0.92 |

Figure 4.34 EDS results for a dust particle

XRD analysis of the dust particles was carried out and with the help of the elements identified in the EDS, different phases in the diffractogram were identified. Figure 4.35 shows the XRD spectrum of the dust sample.

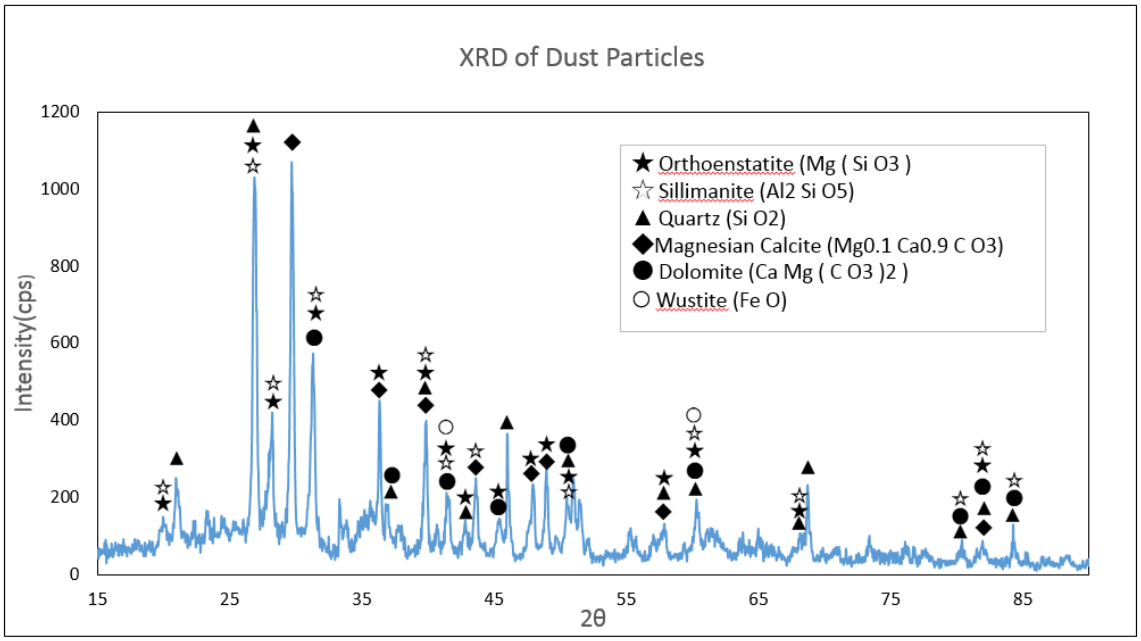


Figure 4.35 X-ray diffractogram of dust particles

The atomic percentage of different phases, as calculated by the Relative Intensity Ratio (RIR Method), is shown in the form a pie chart (Figure 4.36)

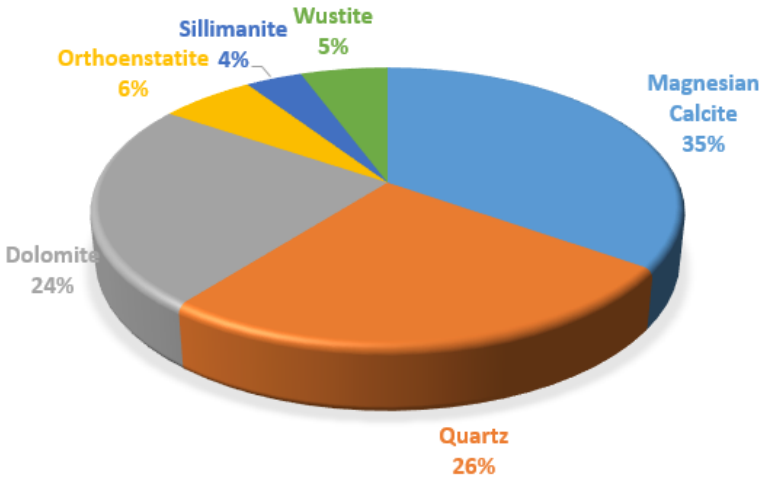


Figure 4.36 Mole percent of different phases of a dust particle

It is evident that the dust particles are mostly composed of Magnesium and Calcium salts. A fair quantity of silica, along-with small percentages of Iron oxide and Aluminum and Magnesium silicates is also present. The theoretical density of the dust particles calculated using the inverse rule of mixture is presented in the Table 4.7.

Table 4.7 Theoretical density calculation for dust particles

| **Phase name** | **Chemical formula** | **Density (kg/m3)** | **Mole Percent** | **Molar Mass (g/mol)** | **Mass Fraction** | **Theoretical Density (kg/m3)** |
|---|---|---|---|---|---|---|
| Magnesian Calcite | Mg0.1 Ca0.9 C O3 | 2740 | 0.35 | 98.43 | 0.31144 | 2864.011833 |
| Quartz | SiO2 | 2620 | 0.26 | 60 | 0.14103 | |
| dolomite HP | Ca Mg ( C O3 )2 | 2840 | 0.24 | 184.4 | 0.40008 | |
| Orthoenstatite | Mg ( Si O3) | 3200 | 0.062 | 100.39 | 0.05627 | |
| Sillimanite | Al2 Si O5 | 3240 | 0.037 | 161.96 | 0.05417 | |
| Wustite | FeO | 5700 | 0.057 | 71.84 | 0.03702 | |

The SEM micrographs indicated the presence of small pores at the surface of the dust particles. Micro-CT analysis of the dust particles was conducted in order to check the distribution of the pores within the dust particle. Table 4.8 highlights the morphometry results as calculated by the Micro CT-Analysis (CT-An) software.

Table 4.8 Morphometry Results for a single dust particle

| **Parameter** | **Unit** | **Value** |
|---|---|---|
| Volume of Dust Particle | $\mu m^3$ | 4316551 |
| Surface Area of Dust Particle | $\mu m^2$ | 1594309 |
| Volume of Closed Pores | $\mu m^3$ | 10432.8 |
| Closed Porosity Percent | % | 0.241 |
| Volume of open Pore Space | $\mu m^3$ | 1162104 |
| Open Porosity Percent | % | 21.0984 |
| Total Porosity Percent | % | 21.2887 |

It is evident from the above results that the particles are in fact porous with a fairly high porosity percentage of 21.28%. Most of the pores, however, are of open nature i.e. they are interconnected and extend all the way to the surface of the particle. The closed pores are the ones that are completely enclosed within the object. The closed porosity percentage is very less in the dust particle. A 3d-cut away model of the dust particle showing the distribution of both the open pores and closed pores is shown in Figure 4.37.

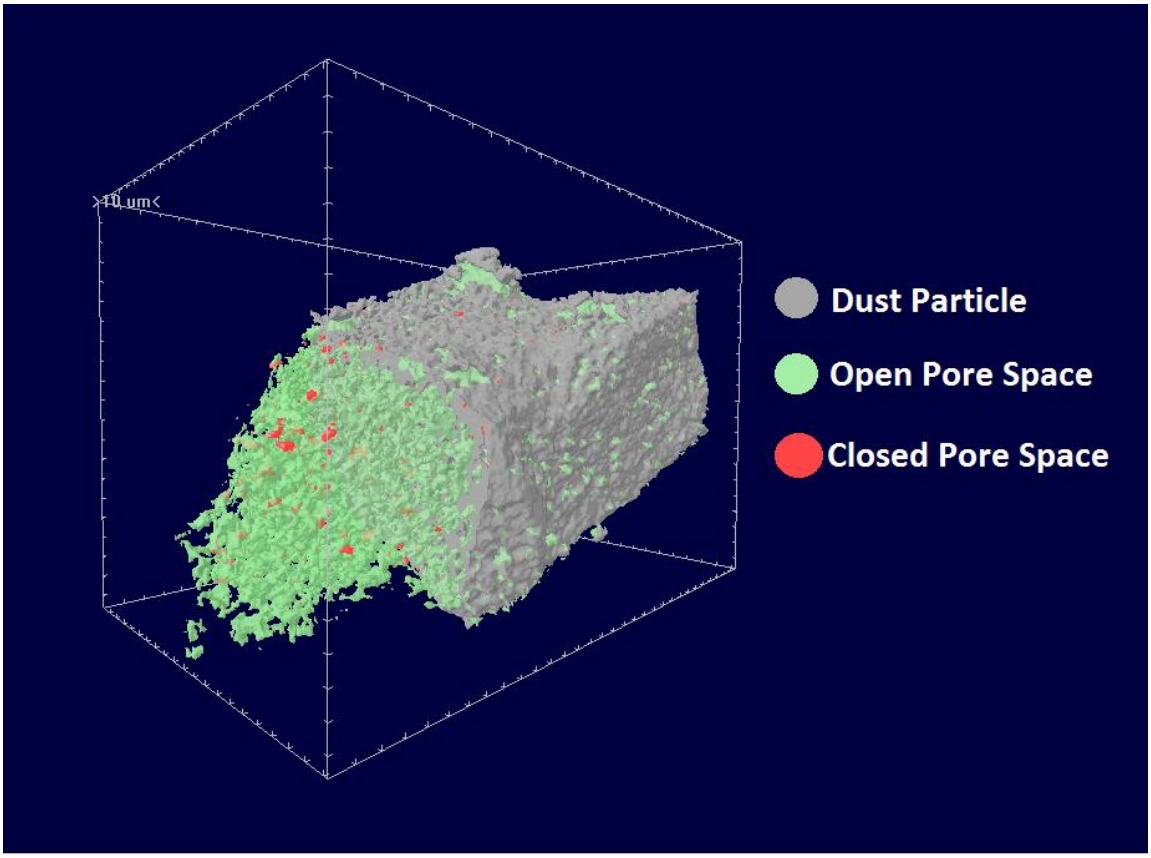


Figure 4.37 3d cut away model for a single dust particle showing open and closed pores

It can be seen from Figure 4.37 that most of the pores are of open nature (highlighted green) i.e. they extend all the way to the surface of the particle. The closed pores (highlighted red) are very small in percentage. It is owing to this interconnected network of open pores that most of the oils are pulled up via capillary action and wet the dust particle upon making contact with.

The last part of the thesis focuses on the interaction of dust particles with a lubricant layer in surfaces impregnated with lubricant oil. It is important to study that how the dust particles in the open environment interact with the lubricant layer. Since silicone oil is used as a lubricant in our study, the focus is on the interaction of dust particles with the silicone

oil. Different sized dust particles were gently placed on silicone oil and it was found that the oil immediately started cloaking the dust particles. Since the dust particles were being wetted by oil, the oil meniscus was elevated and the net surface tension force was acting downwards, thus, further pushing the dust particle into the oil. The density of the dust particles was greater than the silicone oil and, thus, the buoyancy force was not sufficient to support the weight of the particle. Therefore, the dust particles would sink after putting in the silicone oil.

In the second part of this study, the oil was functionalized with PFOTS. The trifluoro methyl (-CF3) groups have a very low surface energy and thus repel oils with low surface tension. After functionalization with PFOTS, the dust particles were again gently placed on silicone oil. This time, the oil was not cloaking the dust particles and the oil meniscus was in fact depressed. The surface tension of the oil was acting upwards to support the weight of the dust particles due to which they remained at the surface of the oil. The functionalized dust particles were later put on the oil impregnated surfaces prepared earlier. Since the lubricant (silicone oil) didn't wet the dust particles, they were easily picked up and carried away by the water droplets. Un-functionalized dust particles, on the other hand, would sink and thus stick to the surface.

# CHAPTER 5

# CONCLUSION

This chapter incudes the conclusions derived from the present study and the findings are presented under the appropriate sections.

## 5.1 Laser Texturing of Alumina Tiles

Alumina surfaces are textured by laser irradiation under high-pressure nitrogen environment. Laser textured surfaces demonstrate superhydrophobic characteristics which is associated with the micro/nano cavities and poles formed at the surface. Since repetitive laser pulses are introduced during laser irradiation of the surface, self-annealing effect is created through heat conduction from the recently formed irradiated spot towards the early formed spot in between the two consecutive pulses. This, in turn, eliminates the crack formation in the laser treated layer. Formation of AlN due to the use of high pressure nitrogen assisting gas reduces the surface energy of the laser treated workpieces.

## 5.2 PDMS Replication of Textured Surfaces

Polydimethylsiloxane (PDMS) is used to copy and replicate laser textured surfaces. PDMS replicated surfaces give similar texture distribution as the laser treated surface. However, some of the detailed sub-micron features, such as fine odd shaped whiskers, are not copied properly from the laser textured surface due to which the contact angle is lower and the

hysteresis for PDMS copied and replicated surfaces is higher than the laser treated surface. Functionalized silica nanoparticles are synthesized by one pot technique [25]. SEM micrographs reveal that the average diameter of the particles is 66nm. FTIR data confirm that the surface of the silica nanoparticles is fully functionalized. In order to improve the wetting characteristics, silica nanoparticles are deposited at the PDMS copied and replicated surfaces. In this case, water droplet contact angle increases and hysteresis reduces considerably. PDMS copied and replicated surfaces have a lower UV/Vis transmittance in comparison to plain PDMS surface. Further small reductions in transmittance are observed after functionalized silica nanoparticles are deposited onto PDMS copied and replicated surfaces.

In the second part of this study, silicon micro post arrays are replicated using PDMS. SEM micrographs reveal that PDMS successfully replicates the micro post array geometry. Replicated PDMS surface with 50 μm post spacing shows the highest contact angle, lowest contact angle hysteresis and a high UV/Vis transmittance. The droplets, however, easily transition from cassie-bexter state to wenzel state for this surface. For replicated micro post array surfaces with post spacing of 25 μm and 10 μm, the cassie-bexter state of the droplet is more stable, though these surfaces have a relatively less CA, high CAH and a comparatively reduced transmittance.

## 5.3 Silica Nanoparticle Coating on Glass

Glass surfaces are made superhydrophobic by coating with a layer of silica nanoparticles. Two different coating strategies, solvent deposition and dip coating are employed. Synthesized silica nano particles are deposited via solvent deposition technique while as-

received silica particles are deposited via dip coating. The CA is high (170°) and the CAH is very low (<1°) for the glass surfaces deposited with synthesized silica nanoparticles. FTIR data reveals the absence of -OH group peak indicating that the surface of the nanoparticles is fully covered with functionalized groups. The SEM micrographs reveal the generation of a hollow porous network formed after solvent deposition of silica nanoparticles which contribute to its superior superhydrophobic properties. The UV/Vis transmittance is relatively low, averaging at 67.22%. The UV/Vis transmittance for the plain glass is around 91.04%.

For the glass surfaces dip coated in silica nanoparticles suspension, the average transmittance is relatively higher, averaging at 83.18%. This is because of the small thickness of the coating. The coating also has small voids which contribute to its higher transmittance. The superhydrophobic characteristics of the coating, on the other hand, are inferior to the one obtained by the solvent deposition of synthesized silica nanoparticles. The is because of a twofold reason. One, the presence of -OH peak in FTIR of the glass surface dip coated with silica particles and functionalized with OTS(Octadecyltrichlorosilane). This suggests the incomplete functionalization of silica particles on by OTS. Second, the presence of large voids in the texture of the glass surface dip coated with silica particles. Due to these factors, the droplet makes contact in wenzel state rather than cassie-bexter state with the surface.

## 5.4 Lubricant Impregnated Surface

The silica coated glass slides are impregnated with silicone oil by slowly pulling them out of an oil bath. The lubricant film stability criterion confirms that the silicone oil film is

stable and completely wets the texture. The silicon oil impregnated surface shows very less water contact angle hysteresis (<1°) and a high UV/Vis transmittance. One undesirable effect is the cloaking of the water droplets by the silicone oil which may lead to lubricant loss as the droplets are shed away.

## 5.5 Dust Characterization

Dust particles, collected from Dhahran, KSA area are characterized using SEM, XRD and Micro-CT. SEM micrographs reveal that the length of the particles vary from 1 μm to over 100 μm. Ellipse fitting on the particles show that the mean particle aspect ratio is 1.37±00.26 while the shape factor is 1.41±0.16. XRD data shows that the dust particles are mostly composed of Magnesian Calcite, followed by Quartz and Dolomite. The density of the dust particles is estimated to be 2864.01 $kg/m^3$. Micro-CT analysis reveals that the dust particles are porous with a total porosity percentage of 21.28%. Most of the pores, however, are of open nature; meaning that they are inter-connected and could be traced all the way back to the surface of the dust particle.

The interaction of dust particles with oil impregnated surfaces is also investigated. It is found that the silicone oil cloaks the dust particle leading to its submersion in the oil. This is an undesirable effect which causes dust accumulation at the lubricant impregnated surfaces. Functionalization of the dust particles, however, makes them stay at the top of the oil. This allows these particles to be picked up and taken away by the water droplets, thus leading to the self-cleaning effect.

## 5.6 Future Works

This thesis presents one of the techniques for the preparation of self-cleaning superhydrophobic surfaces with high optical transparency. The following topics are being suggested as an extension of the current work.

- There is a need to control the coating roughness and the packing behavior of silica nanoparticles during the dip coating process. Selection of dip coating process parameters to obtain the desired surface texture should be investigated. The surface texture can then be optimized to obtain coatings that are superhydrophobic and yet highly optically transparent.
- Performance of self-cleaning surfaces in actual outdoor environments should be evaluated. It should be studied that how well these surfaces perform in removing the accumulated dust particles at the surface. Degradation of the surface superhydrophobic characteristics by exposure to sunlight should also be studied.
- The water droplets normally give a contact angle of around 104° when placed on a lubricant impregnated surface. However, it has been observed that droplets bounce off from the surface when dropped from a certain height. This bouncing behavior of water droplets on lubricant impregnated surfaces should be studied.

# REFERENCES


[1] A. W. Adamson and A. P. (Alice P. Gast, *Physical chemistry of surfaces*. Wiley, 1997.

[2] I. P. Parkin and R. G. Palgrave, "Self-cleaning coatings," *J. Mater. Chem.*, vol. 15, no. 17, p. 1689, 2005.

[3] M. Callies and D. Quéré, "On water repellency," *Soft Matter*, vol. 1, no. 1, pp. 55–61, 2005.

[4] R. F. and, W. Barthlott, C. Neinhuis, and P. Walzel, "Wetting and Self-Cleaning Properties of Artificial Superhydrophobic Surfaces," 2005.

[5] N. Fusetani, "Biofouling and antifouling," *Nat. Prod. Rep.*, vol. 21, no. 1, p. 94, 2004.

[6] P. Muthiah, B. Bhushan, K. Yun, and H. Kondo, "Dual-layered-coated mechanically-durable superomniphobic surfaces with anti-smudge properties," *J. colloid interface*, 2013.

[7] J. Howarter and J. Youngblood, "Self- Cleaning and Next Generation Anti- Fog Surfaces and Coatings," *Macromol. Rapid*, 2008.

[8] G. Bixler and B. Bhushan, "Fluid drag reduction and efficient self-cleaning with rice leaf and butterfly wing bioinspired surfaces," *Nanoscale*, vol. 5, no. 17, p. 7685, 2013.

[9] T. Young, "An Essay on the Cohesion of Fluids," *Philos. Trans. R. Soc. London*, vol. 95, pp. 65–87, 1805.

[10] J. N. Israelachvili, *Intermolecular and surface forces*. Academic Press, 2011.

[11] S. Shibuichi, T. Onda, N. Satoh, and K. Tsujii, "Super Water-repellent Surfaces Resulting from Fractal Structure," *J. Phys. Chem.*, vol. 100, pp. 19512–19517, 1996.

[12] R. N. Wenzel, "RESISTANCE OF SOLID SURFACES TO WETTING BY

WATER," *Ind. Eng. Chem.*, vol. 28, no. 8, pp. 988–994, Aug. 1936.

[13] M. Nosonovsky and B. Bhushan, "Roughness-induced superhydrophobicity: a way to design non-adhesive surfaces," *J. Phys. Condens.*, 2008.

[14] A. B. D. Cassie and S. Baxter, "Wettability of porous surfaces," *Trans. Faraday Soc.*, vol. 40, no. 0, p. 546, 1944.

[15] B. Bhushan, Y. C. Jung, and K. Koch, "Micro-, nano- and hierarchical structures for superhydrophobicity, self-cleaning and low adhesion," *Philos. Trans. R. Soc. London A Math. Phys. Eng. Sci.*, vol. 367, no. 1894, 2009.

[16] N. Michael and B. Bhushan, "Hierarchical roughness makes superhydrophobic states stable," *Microelectron. Eng.*, 2007.

[17] A. Lafuma and D. Quéré, "Superhydrophobic states," *Nat. Mater.*, vol. 2, no. 7, pp. 457–460, Jul. 2003.

[18] T. Deng, K. K. Varanasi, M. Hsu, N. Bhate, C. Keimel, J. Stein, and M. Blohm, "Nonwetting of impinging droplets on textured surfaces," *Appl. Phys. Lett.*, vol. 94, no. 13, p. 133109, 2009.

[19] M. Reyssat, J. M. Yeomans, and D. Quéré, "Impalement of fakir drops," *Epl*, vol. 81, no. 2, p. 26006, Jan. 2008.

[20] L. Bocquet and E. Lauga, "A smooth future?," *Nat. Mater.*, vol. 10, no. 5, pp. 334–337, May 2011.

[21] A. Tuteja, W. Choi, M. Ma, J. M. Mabry, S. A. Mazzella, G. C. Rutledge, G. H. McKinley, and R. E. Cohen, "Designing superoleophobic surfaces.," *Science*, vol. 318, no. 5856, pp. 1618–22, Dec. 2007.

[22] T.-S. Wong, S. H. Kang, S. K. Y. Tang, E. J. Smythe, B. D. Hatton, A. Grinthal, and J. Aizenberg, "Bioinspired self-repairing slippery surfaces with pressure-stable omniphobicity," *Nature*, vol. 477, no. 7365, pp. 443–447, Sep. 2011.

[23] D. Ebert and B. Bhushan, "Transparent, superhydrophobic, and wear-resistant coatings on glass and polymer substrates using SiO2, ZnO, and ITO nanoparticles,"

*Langmuir*, vol. 28, no. 31, pp. 11391–11399, Aug. 2012.

[24] X. Yao, Y. Hu, A. Grinthal, T.-S. Wong, L. Mahadevan, and J. Aizenberg, "Adaptive fluid-infused porous films with tunable transparency and wettability," *Nat. Mater.*, vol. 12, no. 6, pp. 529–534, Apr. 2013.

[25] W. Y. D. Yong, Z. Zhang, G. Cristobal, and W. S. Chin, "One-pot synthesis of surface functionalized spherical silica particles," *Colloids Surfaces A Physicochem. Eng. Asp.*, vol. 460, pp. 151–157, 2014.

[26] J. D. Smith, R. Dhiman, S. Anand, E. Reza-Garduno, R. E. Cohen, G. H. McKinley, and K. K. Varanasi, "Droplet mobility on lubricant-impregnated surfaces," *Soft Matter*, vol. 9, no. 6, pp. 1772–1780, 2013.

[27] B. S. Yilbas, A. Matthews, C. Karatas, A. Leyland, M. Khaled, N. Abu-Dheir, N. Al-Aqeeli, and X. Nie, "Laser Texturing of Plasma Electrolytically Oxidized Aluminum 6061 Surfaces for Improved Hydrophobicity," *J. Manuf. Sci. Eng.*, vol. 136, no. 5, p. 54501, Aug. 2014.

[28] B. S. Yilbas, "Laser texturing of zirconia surface with presence of TiC and B4C: Surface hydrophobicity, metallurgical, and mechanical characteristics," *Ceram. Int.*, vol. 40, no. 10, pp. 16159–16167, 2014.

[29] G. Azimi, H.-M. Kwon, and K. K. Varanasi, "Superhydrophobic surfaces by laser ablation of rare-earth oxide ceramics," *MRS Commun.*, vol. 4, no. 3, pp. 1–5, Sep. 2014.

[30] D. Triantafyllidis, L. Li, and F. H. Stott, "Surface treatment of alumina-based ceramics using combined laser sources," *Appl. Surf. Sci.*, vol. 186, no. 1, pp. 140–144, 2002.

[31] B. S. Yilbas, C. Karatas, A. F. M. Arif, and B. J. A. Aleem, "Laser gas assisted nitriding of alumina surfaces," *Surf. Eng.*, vol. 25, no. 3, pp. 235–240, Apr. 2009.

[32] B. S. Yilbas, M. Khaled, N. Abu-Dheir, N. Aqeeli, and S. Z. Furquan, "Laser texturing of alumina surface for improved hydrophobicity," *Appl. Surf. Sci.*, vol. 286, pp. 161–170, 2013.

[33] R. Jagdheesh, “Fabrication of a Superhydrophobic Al2O3 Surface Using Picosecond Laser Pulses,” *Langmuir*, vol. 30, no. 40, pp. 12067–12073, Oct. 2014.

[34] V. D. Ta, A. Dunn, T. J. Wasley, J. Li, R. W. Kay, J. Stringer, P. J. Smith, E. Esenturk, C. Connaughton, and J. D. Shephard, “Laser textured superhydrophobic surfaces and their applications for homogeneous spot deposition,” *Appl. Surf. Sci.*, vol. 365, pp. 153–159, 2016.

[35] D. V. Ta, A. Dunn, T. J. Wasley, R. W. Kay, J. Stringer, P. J. Smith, C. Connaughton, and J. D. Shephard, “Nanosecond laser textured superhydrophobic metallic surfaces and their chemical sensing applications,” *Appl. Surf. Sci.*, vol. 357, pp. 248–254, 2015.

[36] G. Shao, J. Wu, Z. Cai, and W. Wang, “Fabrication of elastomeric high-aspect-ratio microstructures using polydimethylsiloxane (PDMS) double casting technique,” *Sensors Actuators A Phys.*, vol. 178, pp. 230–236, 2012.

[37] L. Yang, X. Hao, C. Wang, B. Zhang, and W. Wang, “Rapid and low cost replication of complex microfluidic structures with PDMS double casting technology,” *Microsyst. Technol.*, vol. 20, no. 10–11, pp. 1933–1940, Oct. 2014.

[38] L. Gitlin, P. Schulze, and D. Belder, “Rapid replication of master structures by double casting with PDMS,” *Lab Chip*, vol. 9, no. 20, p. 3000, Oct. 2009.

[39] J. Yeo and D. S. Kim, “The effect of the aspect ratio on the hydrophobicity of microstructured polydimethylsiloxane (PDMS) robust surfaces,” *Microsyst. Technol.*, vol. 16, no. 8–9, pp. 1457–1463, Aug. 2010.

[40] M. Adithyavairavan and S. Subbiah, “A morphological study on direct polymer cast micro-textured hydrophobic surfaces,” *Surf. Coatings Technol.*, vol. 205, no. 20, pp. 4764–4770, 2011.

[41] Y.-C. Lin, S.-H. Hsu, and Y.-C. Chung, “Thermal imprint techniques for preparation of superhydrophobic polymer coatings,” *Surf. Coatings Technol.*, vol. 231, pp. 501–506, 2013.

[42] T. O. Yoon, H. J. Shin, S. C. Jeoung, and Y.-I. Park, “Formation of

superhydrophobic poly(dimethysiloxane) by ultrafast laser-induced surface modification," *Opt. Express*, vol. 16, no. 17, p. 12715, Aug. 2008.

[43] W. Stöber, A. Fink, and E. Bohn, "Controlled growth of monodisperse silica spheres in the micron size range," *J. Colloid Interface Sci.*, vol. 26, no. 1, pp. 62–69, 1968.

[44] G. H. Bogush, M. A. Tracy, and C. F. Zukoski, "Preparation of monodisperse silica particles: Control of size and mass fraction," *J. Non. Cryst. Solids*, vol. 104, no. 1, pp. 95–106, 1988.

[45] I. A. M. Ibrahim, A. A. F. Zikry, M. A. Sharaf, and A. Zikry, "Preparation of spherical silica nanoparticles: Stober silica," *J. Am. Sci.*, vol. 66985989, no. 1111, pp. 1545–1003, 2010.

[46] X.-D. Wang, Z.-X. Shen, T. Sang, X.-B. Cheng, M.-F. Li, L.-Y. Chen, and Z.-S. Wang, "Preparation of spherical silica particles by Stöber process with high concentration of tetra-ethyl-orthosilicate," *J. Colloid Interface Sci.*, vol. 341, no. 1, pp. 23–29, 2010.

[47] T. I. Suratwala, M. L. Hanna, E. L. Miller, P. K. Whitman, I. M. Thomas, P. R. Ehrmann, R. S. Maxwell, and A. K. Burnham, "Surface chemistry and trimethylsilyl functionalization of Stöber silica sols," *J. Non. Cryst. Solids*, vol. 316, no. 2, pp. 349–363, 2003.

[48] J. Bravo, L. Zhai, Z. Wu, R. E. Cohen, and M. F. Rubner, "Transparent superhydrophobic films based on silica nanoparticles," *Langmuir*, vol. 23, no. 13, pp. 7293–7298, 2007.

[49] X. Y. Ling, I. Y. Phang, G. J. Vancso, J. Huskens, and D. N. Reinhoudt, "Stable and transparent superhydrophobic nanoparticle films," *Langmuir*, vol. 25, no. 5, pp. 3260–3263, Mar. 2009.

[50] Y. Li, F. Liu, and J. Sun, "A facile layer-by-layer deposition process for the fabrication of highly transparent superhydrophobic coatings.," *Chem. Commun. (Camb).*, vol. 14, no. 19, pp. 2730–2732, 2009.

[51] H. Ogihara, J. Xie, and T. Saji, "Controlling surface energy of glass substrates to

prepare superhydrophobic and transparent films from silica nanoparticle suspensions," 2015.

[52] A. K. Epstein, T.-S. Wong, R. A. Belisle, E. M. Boggs, and J. Aizenberg, "Liquid-infused structured surfaces with exceptional anti-biofouling performance.," *Proc. Natl. Acad. Sci. U. S. A.*, vol. 109, no. 33, pp. 13182–7, Aug. 2012.

[53] X. Huang, J. D. Chrisman, and N. S. Zacharia, "Omniphobic Slippery Coatings Based on Lubricant-Infused Porous Polyelectrolyte Multilayers," *ACS Macro Lett.*, vol. 2, no. 9, pp. 826–829, Sep. 2013.

[54] P. Kim, M. J. Kreder, J. Alvarenga, and J. Aizenberg, "Hierarchical or Not? Effect of the Length Scale and Hierarchy of the Surface Roughness on Omniphobicity of Lubricant-Infused Substrates," *Nano Lett.*, vol. 13, no. 4, pp. 1793–1799, Apr. 2013.

[55] S. Anand, A. T. Paxson, R. Dhiman, J. D. Smith, and K. K. Varanasi, "Enhanced condensation on lubricant-impregnated nanotextured surfaces," *ACS Nano*, vol. 6, no. 11, pp. 10122–10129, Nov. 2012.

[56] P. Kim, T.-S. Wong, J. Alvarenga, M. J. Kreder, W. E. Adorno-Martinez, and J. Aizenberg, "Liquid-Infused Nanostructured Surfaces with Extreme Anti-Ice and Anti-Frost Performance," *ACS Nano*, vol. 6, no. 8, pp. 6569–6577, Aug. 2012.

[57] B. S. Yilbas, S. S. Akhtar, and C. Karatas, "Laser gas assisted melting of preprepared alumina surface including TiC particles at surface," *Surf. Eng.*, vol. 27, no. 6, pp. 470–476, Jul. 2011.

[58] Z. Huang, S. Cho, D. Jiang, and S. Tan, "Surface nitridation of Al2O3 based composite by N2-HIP post-treatment," *J. Mater. Sci.*, vol. 34, no. 9, pp. 2023–2027, 1999.

[59] A. L. Ji, L. B. Ma, C. Liu, C. R. Li, and Z. X. Cao, "Synthesis and characterization of superhard aluminum carbonitride thin films," *Diam. Relat. Mater.*, vol. 14, no. 8, pp. 1348–1352, 2005.

[60] C. J. van Oss, R. J. Good, and R. J. Busscher, "ESTIMATION OF THE POLAR SURFACE TENSION PARAMETERS OF GLYCEROL AND FORMAMIDE,

FOR USE IN CONTACT ANGLE MEASUREMENTS ON POLAR SOLIDS," *J. Dispers. Sci. Technol.*, vol. 11, no. 1, pp. 75–81, Feb. 1990.

[61] F. Schneider, J. Draheim, R. Kamberger, and U. Wallrabe, "Process and material properties of polydimethylsiloxane (PDMS) for Optical MEMS," *Sensors Actuators A Phys.*, vol. 151, no. 2, pp. 95–99, 2009.

[62] A. van Blaaderen and A. P. M. Kentgens, "Particle morphology and chemical microstructure of colloidal silica spheres made from alkoxysilanes," *J. Non. Cryst. Solids*, vol. 149, no. 3, pp. 161–178, 1992.

[63] J. Lin, H. Chen, Y. Ji, and Y. Zhang, "Functionally modified monodisperse core–shell silica nanoparticles: Silane coupling agent as capping and size tuning agent," *Colloids Surfaces A Physicochem. Eng. Asp.*, vol. 411, pp. 111–121, 2012.

[64] N. J. Shirtcliffe, G. McHale, M. I. Newton, G. Chabrol, and C. C. Perry, "Dual-Scale Roughness Produces Unusually Water-Repellent Surfaces," *Adv. Mater.*, vol. 16, no. 21, pp. 1929–1932, Nov. 2004.

[65] K. R. Aguiar, V. G. Santos, M. N. Eberlin, K. Rischka, M. Noeske, G. Tremiliosi-Filho, and U. P. Rodrigues-Filho, "Efficient green synthesis of bis(cyclic carbonate)poly(dimethylsiloxane) derivative using CO2 addition: a novel precursor for synthesis of urethanes," *RSC Adv.*, vol. 4, no. 46, p. 24334, 2014.

[66] A. L. (Albert L. Smith, *The Analytical chemistry of silicones*. Wiley, 1991.

[67] S. H. Kim, M. T. (Michael T. . Dugger, and K. L. Mittal, *Adhesion aspects in MEMS-NEMS*. Brill, 2010.

[68] B. G. Prevo, Y. Hwang, and O. D. Velev, "Convective Assembly of Antireflective Silica Coatings with Controlled Thickness and Refractive Index," *Chem. Mater.*, vol. 17, no. 14, pp. 3642–3651, Jul. 2005.

[69] H. B. Eral, D. M. Augustine, M. H. G. Duits, and F. Mugele, "Suppressing the coffee stain effect: how to control colloidal self-assembly in evaporating drops using electrowetting," *Soft Matter*, vol. 7, no. 10, p. 4954, 2011.

[70] Y. S. Chaudhary, J. Ghatak, U. M. Bhatta, and D. Khushalani, “One-step method for the self-assembly of metal nanoparticles onto facetted hollow silica tubes,” *J. Mater. Chem.*, vol. 16, no. 36, p. 3619, 2006.

[71] D.-J. Yun and S.-W. Rhee, “Self-Assembled Monolayer Formation on Molybdenum with Octadecyltrichlorosilane and Phenethyltrichlorosilane and Measurement of Molybdenum–Pentacene Interface Properties,” *J. Electrochem. Soc.*, vol. 155, no. 6, p. H357, 2008.

# Vitae

| | |
|---|---|
| Name | :Muhammad Rizwan Yousaf |
| Nationality | :Pakistani |
| Date of Birth | :9/15/1990 |
| Email | :rizwangiki@gmail.com |
| Address | : House#1088, St#5, Ph-2 Ext., Bahria Town, Rawalpindi, Pakistan |
| Academic Background | :**MS Mechanical Engineering**<br>Jan 2016<br>King Fahd University of Petroleum and Minerals<br>Dhahran, Saudi Arabia<br>**BS Mechanical Engineering**<br>June, 2013<br>Ghulam Ishaq Khan Institute of Engineering Sciences and Technology, Swabi, Pakistan |
| Publications | **:** Yilbas, Bekir Sami, M. Rizwan Yousaf, H. Ali, and N. Al‐Aqeeli. "Replication of laser‐textured alumina surfaces by polydimethylsiloxane: Improvement of surface hydrophobicity." Journal of Applied Polymer Science 133, no. 41 (2016). |